Neuroscience 330 (2016) 267–290

THE INTERCALATED NUCLEAR COMPLEX OF THE PRIMATE AMYGDALA

BASILIS ZIKOPOULOS,[a,b]* YOHAN J. JOHN,[c] MIGUEL ÁNGEL GARCÍA-CABEZAS,[c] JAMIE G. BUNCE[c] AND HELEN BARBAS[b,c]

[a] *Human Systems Neuroscience Laboratory, Department of Health Sciences, Boston University, Boston, MA, United States*

[b] *Graduate Program for Neuroscience, Boston University and School of Medicine, Boston, MA, United States*

[c] *Neural Systems Laboratory, Department of Health Sciences, Boston University, Boston, MA, United States*

Abstract—The organization of the inhibitory intercalated cell masses (IM) of the primate amygdala is largely unknown despite their key role in emotional processes. We studied the structural, topographic, neurochemical and intrinsic connectional features of IM neurons in the rhesus monkey brain. We found that the intercalated neurons are not confined to discrete cell clusters, but form a neuronal net that is interposed between the basal nuclei and extends to the dorsally located anterior, central, and medial nuclei of the amygdala. Unlike the IM in rodents, which are prominent in the anterior half of the amygdala, the primate inhibitory net stretched throughout the antero-posterior axis of the amygdala, and was most prominent in the central and posterior extent of the amygdala. There were two morphologic types of intercalated neurons: spiny and aspiny. Spiny neurons were the most abundant; their somata were small or medium size, round or elongated, and their dendritic trees were round or bipolar, depending on location. The aspiny neurons were on average slightly larger and had varicose dendrites with no spines. There were three non-overlapping neurochemical populations of IM neurons, in descending order of abundance: (1) Spiny neurons that were positive for the striatal associated dopamine- and cAMP-regulated phosphoprotein (DARPP-32+); (2) Aspiny neurons that expressed the calcium-binding protein calbindin (CB+); and (3) Aspiny neurons that expressed nitric oxide synthase (NOS+). The unique combinations of structural and neurochemical features of the three classes of IM neurons suggest different physiological properties and function. The three types of IM neurons were intermingled and likely interconnected in distinct ways, and were innervated by intrinsic neurons within the amygdala, or by external sources, in pathways that underlie fear conditioning and anxiety.

Key words: emotion, inhibition, connectivity, quantitative anatomy, medium spiny, anxiety.

INTRODUCTION

The amygdala is a central node in the brain's emotional system, involved in aspects of affective learning, memory and response generation (Phelps, 2006; Murray, 2007; Pessoa, 2008; Morrison and Salzman, 2010; Pape and Pare, 2010; Pessoa and Adolphs, 2010; John et al., 2013; Paz and Pare, 2013; Lalumiere, 2014). The amygdala has also been implicated in pathological states including neuropsychiatric disorders and drug addiction (Heimer, 2003; Phillips et al., 2003; Quirk and Gehlert, 2003; Shin et al., 2006; Murray et al., 2011; Tye et al., 2011; Maren et al., 2013; Likhtik and Paz, 2015).

Diverse amygdalar functions and dysfunction have been linked to three functional groups of nuclei that have specialized connectivity patterns, each associated with distinct networks (De Olmos et al., 1985; De Olmos, 1990; De Olmos and Heimer, 1999; Sah et al., 2003; Waclaw et al., 2010; John et al., 2013): (1) a large group consists of nuclei connected with the cerebral cortex and includes the cortical nuclei (Co), and the basal amygdala (BA), which is further subdivided into the basolateral (BL), basomedial (BM, also known as accessory basal) and lateral (La) nuclei; (2) nuclei with neurons that resemble striatal neurons, consisting of the central (Ce) and medial (Me) nuclei, which innervate hypothalamic and brainstem autonomic centers; (3) and the intercalated nuclei, islands, clusters, or masses (IM), which consist of inhibitory neurons that are interposed between the other two major groups of amygdalar nuclei.

The amygdala is enriched with a large variety of local inhibitory neurons, some of which resemble cortical inhibitory neurons, and others, like the IM, which are striatal-like. Cortical-like inhibitory interneurons are found in the basal, lateral and cortical nuclei, as well as the amygdalohippocampal area, and resemble GABAergic neurons of the cortex, based on similar firing

*Correspondence to: B. Zikopoulos, Human Systems Neuroscience Laboratory, Department of Health Sciences, Boston University, Boston, MA, United States.
E-mail address: zikopoul@bu.edu (B. Zikopoulos).

Abbreviations: AChE, acetylcholinesterase; BA or BLA, basolateral nuclear complex; BL, basolateral nucleus; BM, basomedial nucleus; CB, calbindin; Ce, central nucleus; CeL, lateral subdivision of the central nucleus; CeM, medial subdivision of the central nucleus; Co, cortical nuclei; CR, calretinin; D1, dopamine receptor 1; DARPP-32, dopamine and cAMP-regulated phosphoprotein; EM, electron microscopy; GABA, gamma-Aminobutyric acid; GAD67, L-glutamic acid decarboxylase 67; IM, intercalated nuclei, islands, clusters, or masses; ITC, intercalated cells or clusters; ITCd, intercalated cells or clusters, dorsolateral group; ITCv, intercalated cells or clusters, ventromedial group; La, lateral nucleus; Me, medial nucleus; NADPHd, β-nicotinamide adenine dinucleotide phosphate diaphorase; NO, nitric oxide; NOS, nitric oxide synthase; PSD, post-synaptic density; PV, parvalbumin; Thr, threonine.

http://dx.doi.org/10.1016/j.neuroscience.2016.05.052
0306-4522/

patterns, neurochemical markers and synaptic specificity with dendritic, somatic, or axonal elements of nearby pyramidal neurons [reviewed in (Capogna, 2014)]. Striatal-like inhibitory neurons are found primarily in IM, Ce, Me, and Co and morphologically resemble medium-sized spiny striatal neurons (Millhouse, 1986; De Olmos, 1990; Urban and Yilmazer-Hanke, 1999; Marcellino et al., 2012). The diversity of inhibitory neurons suggests that inhibition is a critical regulator of activity in the amygdala (Quirk and Gehlert, 2003; Pape, 2005; Duvarci and Pare, 2014; Wolff et al., 2014) that likely accounts for the low spontaneous firing rates of neurons in the lateral and central nuclei [reviewed in (Pare et al., 2003; Quirk and Gehlert, 2003; Pape, 2005)]. Interfering with normal inhibition in the amygdala can lead to elevated local activity, which is associated with anxiety-related behaviors and disruption of fear extinction [reviewed in (Quirk and Gehlert, 2003)]. It is therefore crucial to understand key groups of neurons that facilitate inhibitory regulation in the amygdala.

The inhibitory IM neurons play a central role in the regulation of the activity of the amygdala. Several studies have pointed to the unique positioning of IM neurons, their inhibitory nature and complex connectivity patterns, and have demonstrated their central role in circuits involved in fear conditioning, extinction, complex emotional processes and anxiety (Royer et al., 1999; Pare et al., 2004; Likhtik et al., 2008; Busti et al., 2011; Palomares-Castillo et al., 2012). As key nodes of these circuits, IM neurons receive direct excitatory input from the cortex, thalamus, and basal and lateral amygdalar nuclei (Millhouse, 1986; Ghashghaei and Barbas, 2002; Amano et al., 2010; Barbas et al., 2011; Marcellino et al., 2012; Pinard et al., 2012; Asede et al., 2015; Strobel et al., 2015). In turn, IM neurons send inhibitory projections to other IM neurons, and to the output of the amygdala, including the basal (BM, BL), lateral (La), and the inhibitory central (Ce) and medial (Me) nuclei, modulating emotional responses (Millhouse, 1986; Pare and Smith, 1993; Royer et al., 2000b; Amano et al., 2010; Manko et al., 2011).

Most detailed accounts of IM nuclei in the literature are in rodents (De Olmos et al., 1985; Millhouse, 1986; Manko et al., 2011; Marcellino et al., 2012). The organization of the IM nuclei in primates is largely unexplored, and limited to reports highlighting their considerable variability in morphology, numbers and density (Crosby and Humphrey, 1941; Stephan and Andy, 1977; De Olmos, 1990; Urban and Yilmazer-Hanke, 1999; Carlo et al., 2010). To address this issue, we studied the structural and neurochemical features of histochemically and immunohistochemically labeled IM neurons in the rhesus monkey brain, and mapped their distribution quantitatively. In addition, we examined the ultrastructural and neurochemical features of synapses in the IM neuropil to investigate the innervation of IM neurons by excitatory and inhibitory inputs. Our results highlight important features of inhibitory IM neurons and their circuits in a primate species and suggest novel mechanisms that may underlie their unique functional specialization in processing emotions and learning.

EXPERIMENTAL PROCEDURES

We used brain tissue from sixteen male and female rhesus monkeys (*Macaca mulatta*, ages ranging from 2.5 to 4 years). We double and triple immunolabeled coronal sections through the primate amygdala (Fig. 1), to co-visualize markers of inhibitory neurons, including gamma-Aminobutyric acid (GABA) or L-glutamic acid decarboxylase 67 (GAD67) with nitric oxide synthase (NOS) or β-nicotinamide adenine dinucleotide phosphate diaphorase (NADPHd), calcium-binding proteins calbindin (CB), calretinin (CR), or parvalbumin (PV), and dopamine and cAMP-regulated phosphoprotein (DARPP-32). We also mapped nuclei in the amygdala and stereologically quantified the number and density of IM neurons using Nissl-stained sections or markers of inhibitory neurons. We used 3D-analysis and reconstruction to study the distribution of distinct types of inhibitory neurons at the light and confocal

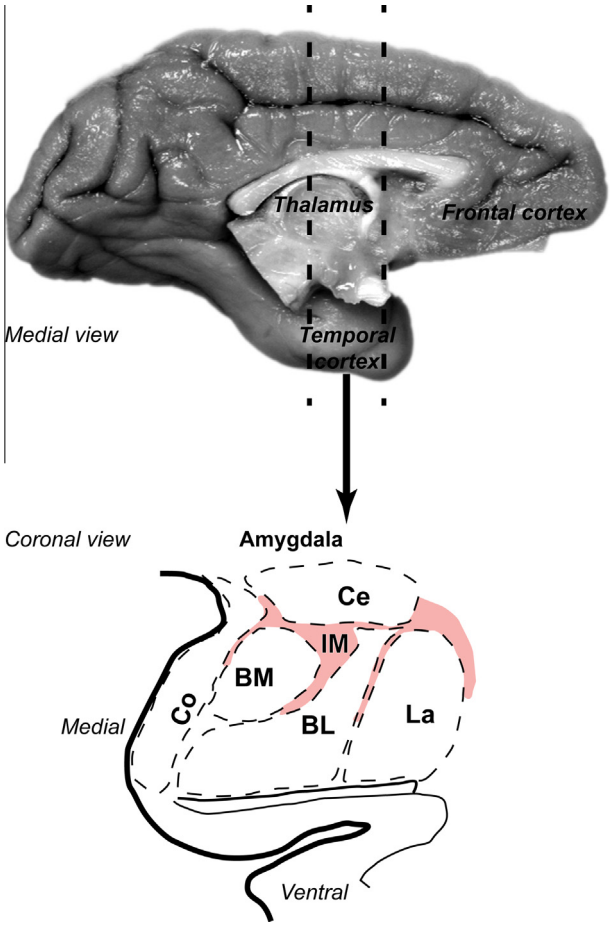

Fig. 1. The rhesus macaque amygdala. Medial view (top) of the rhesus monkey brain shows the temporal region that contains the primate amygdala (dotted lines). Bottom panel shows coronal view of the outline of a representative section through a central level of the antero-posterior extent of the amygdala. Pink hue delineates the extensive regions between amygdalar nuclei that contain IM clusters and numerous, previously unclassified inhibitory neurons. This area was collectively designated as IM in the primate amygdala. (For interpretation of the references to colour in this figure legend, the reader is referred to the web version of this article.)

microscope, and 3D-serial electron microscopy (EM) to study synaptic features in IM.

Animals and tissue preparation

Animals were obtained through the New England Primate Research Center (1 Pinehill Rd, Southborough, MA 01772, USA). Procedures were designed to minimize animal suffering and to reduce the number of animals used. As a result, all animals used in this study were also used in other, unrelated tract-tracing studies. Detailed protocols of the procedures were approved by the Institutional Animal Care and Use Committee at Harvard Medical School and Boston University School of Medicine in accordance with NIH guidelines (DHEW Publication no. [NIH] 80-22,, revised 1996, Office of Science and Health Reports, DRR/NIH, Bethesda, MD, USA).

For transcardial perfusion animals were deeply anesthetized with a lethal dose of sodium pentobarbital (>50 mg/kg, intravenous, to effect) according to one of the following protocols. One group of animals ($n = 3$) was transcardially perfused with saline followed by 4% ($n = 1$) or 6% ($n = 2$) paraformaldehyde in cacodylate buffer (0.1 M at pH 7.4) and postfixed in a solution of 4% or 6% paraformaldehyde in glycerol phosphate buffer [10% glycerol and 2% dimethyl sulfoxide (DMSO) in PB 0.1 M at pH 7.4]. The rest of the animals ($n = 13$) were transcardially perfused with saline followed by 4% paraformaldehyde in PB (0.1 M at pH 7.4); for a subset from this group ($n = 7$) the fixative also included 0.2% glutaraldehyde, needed for electron microscopic study.

After removal from the skull brains were photographed, cryoprotected in a series of sucrose solutions (10–30% in 0.01 M PBS) and frozen in −75 °C isopentane (Fisher Scientific, Pittsburg, PA, USA) for rapid and uniform freezing (Rosene et al., 1986). Brains were cut in the coronal plane on a freezing microtome at 40 or 50 μm to produce ten matched series. To preserve the ultrastructure, the rest of the tissue was stored until processing in −20 °C in anti-freeze solution (30% ethylene glycol, 30% glycerol, 40% 0.05 M PB, pH 7.4 with 0.05% azide).

Histochemistry, histo-enzymatic staining, and immunohistochemistry

To delineate the borders of the nuclei of the amygdala we stained adjacent series of sections for Nissl, using either thionin or cresyl violet (cases AJ, AN, AQ, AW, BC, BO), and myelin (cases AJ, AN, AQ, AW) or acetylcholinesterase (AChE; cases AJ, AN, AQ, AW), as described previously (Barbas and De Olmos, 1990). For Nissl staining, sections were mounted on chrome-alum-coated slides, dried, defatted in a 1:1 solution of chloroform and 100% ethanol for 1 h, rehydrated through a series of graded alcohols and distilled water, stained with 0.05% thionin (pH 4.5) or 0.1% cresyl violet (pH 3.8) for 3–15 min and differentiated through graded alcohols and xylenes. Sections were coverslipped with mounting media (Permount, Fisher Scientific, Pittsburg, PA, USA; or Entellan, Electron Microscopy Sciences, Hatfield, PA, USA).

We stained myelin using the Gallyas silver stain. Briefly, sections were rinsed in distilled water and then incubated in a solution of pyridine (2/3; P368-1 Fischer Scientific) and glacial acetic acid (1/3; ARK2183 Sigma–Aldrich) for 30 min at room temperature. Sections were washed again in distilled water followed by incubation in the impregnation solution for a minimum of 30 min at room temperature in the dark. Impregnation solution consisted of 0.1 g ammonium nitrate (A7455 Sigma–Aldrich) and 0.1-g silver nitrate (S181-25 Fischer Scientific) per 100 ml of distilled water; the pH of the solution was adjusted with 0.1 M sodium hydroxide (CAS 1: 1310-73-2 Fischer Scientific) to obtain pH 7.5. After rinses in 0.5% acetic acid (A6283 Sigma–Aldrich) sections were incubated in the developing solution under microscopic control until the proper level of stain was achieved. The developing solution was a mix of the following three solutions (each dissolved in 500 ml of distilled water): A, 25-g sodium carbonate (S-263 Fischer Scientific); B, 1-g ammonium nitrate (A7455 Sigma–Aldrich), 1-g silver nitrate (S181-25 Fischer Scientific) and 5-g silico-tungstic acid (383341 Sigma–Aldrich); C, 75 ml of solution B and 1.75 ml of 4% paraformaldehyde (O4042 Fischer Scientific). The incubation solution was made by mixing 150 ml of solution A, 75 ml of solution B and 75 ml of solution C in that order. After developing, the sections were washed in 1% acetic acid (A6283 Sigma–Aldrich) and then in distilled water followed by incubation in 5% sodium thiosulfate (S-1648 Sigma–Aldrich) to stabilize the reaction. Sections were finally washed in distilled water and mounted in PB 0.1 M, pH 7.4.

For AChE staining we rinsed sections in distilled water and then incubated them overnight at 4 °C in the dark in a solution prepared from the combination of the following five compounds (each dissolved in 200 ml of distilled water): 72-mg ethopropazine hydrochloride (E5406 Sigma–Aldrich, St. Louis, MO), 1.156-mg acetylthiocholine iodide (A5751 Sigma–Aldrich), 750 mg of glycine (BP381 Fischer Scientific, Fair Lawn, NJ, USA), 500 mg of cupric sulfate (C-493 Fischer Scientific) and 6.8 mg of sodium acetate (S-209 Fischer Scientific). The pH was adjusted with acetic acid (A6283, Sigma–Aldrich) to reach pH 5.0. Sections were then rinsed six times in distilled water followed by incubation for 2 min at room temperature in the dark in sodium sulfide solution [19.2 g of sodium sulfide (407410 Sigma–Aldrich) in 450 ml of 0.1 N HCl; pH was adjusted with 10 N HCl (7647-01-0 Fischer Scientific) to pH 7.8 and the final solution was made by adding 500 ml of distilled water]. Sections were then rinsed in distilled water and developed in silver nitrate solution [5 g of silver nitrate (S181-25 Fischer Scientific) in 500 ml of distilled water] for 2 min at room temperature in the dark until the proper level of stain was achieved. Finally, sections were rinsed in distilled water and then in 0.1 M PB pH7.4 and mounted on gelatin coated slides.

We stained sections for NADPHd (cases AN, AQ), which is a good marker for NOS in the mammalian

central nervous system (Hope et al., 1991; Hashikawa et al., 1994). We stained free floating sections containing the amygdala, as described (Dombrowski and Barbas, 1996). Free-floating sections were washed in 0.1 M Tris–HCl buffer (pH 7.4, 37 °C), incubated at 40 °C in the same buffer containing 0.8 mM β-nicotinamide adenine dinucleotide phosphate, reduced form (NADPH, Sigma–Aldrich N-1630), 0.8 mM Nitro Blue Tetrazolium (Sigma–Aldrich N-6876), 0.1% Triton-X and 0.16% malic acid for 60–90 min in constant agitation. Sections were washed in 0.1 M Tris–HCl buffer, mounted on gelatin-coated slides, dried, counterstained with 1% Neutral Red solution, dehydrated, cleared and coverslipped with Permount (Fisher Scientific).

For immunoperoxidase histochemistry, free-floating sections were rinsed in 0.01 M PBS, incubated in 0.05 M glycine, pre-blocked in 10% normal goat serum (NGS) and 5% bovine serum albumin (BSA) with 0.2% Triton-X for 1 h and incubated overnight in primary antibody against GABA (rabbit anti-GABA, diluted 1:1,000; ImmunoStar, or mouse anti-GABA, diluted 1:100, Sigma–Aldrich; cases BK, BO), GAD67 (mouse anti-GAD67, diluted 1:200, Millipore, Billerica MA USA; cases AW, BK), neuronal nuclear antigen (NeuN, mouse anti-NeuN, diluted 1:200, Millipore; cases BB, BD), **d**opamine- and c**A**MP-**r**egulated **p**hospho**p**rotein, of $\boldsymbol{M}_r$ **32**,000 (DARPP-32, mouse anti-DARPP-32, diluted 1:30,000, generous gift from Drs. Paul Greengard and Jean-Antoine Girault; cases AJ, AL, AN, AQ, BK, BL, BN, BR), nitric oxide synthase (NOS, mouse anti-nNOS, diluted 1:400, BD Transduction Labs, San Jose CA, or rabbit anti-nNOS, diluted 1:400, Millipore; cases BI, BL, BN, BR), dopamine receptor 1 (D1, rat anti-D1, diluted 1:800, Sigma–Aldrich; case BR), and the calcium binding proteins parvalbumin (PV, mouse anti-PV, diluted 1:2,000, Swant Antibodies, Switzerland; cases AZ, BK), calbindin (CB, mouse anti-CB or rabbit anti-CB, diluted 1:2,000, Swant Antibodies, Switzerland; cases AX, AZ, BB, BC, BI, BK, BL, BN, BR) and calretinin (CR, mouse anti-CR or rabbit anti-CR, diluted 1:2,000, Swant Antibodies, Switzerland; case BK). Sections were then rinsed in PBS and incubated for 4 h in secondary biotinylated goat anti-mouse IgG or anti-rat IgG or mouse anti-rabbit IgG (1:200, in PBS, 1% NGS, 1% BSA, 0.1% Triton-X, Vector Laboratories, Burlingame, CA, USA), followed by 1 h in an avidin–biotin horseradish peroxidase complex (AB-HRP kit; Vectastain PK-6100 ABC Elite kit, Vector Laboratories, Burlingame, CA, USA; diluted 1:100 in 0.01 M PBS with 0.1% Triton X-100). Sections were rinsed and processed for 2–3 min for the peroxidase-catalyzed polymerization of diaminobenzidine (DAB; DAB kit, Vector Laboratories or Zymed Laboratories Inc., South San Francisco, CA, USA; 0.05% DAB, and 0.004% H_2O_2 in PBS).

For double immunofluorescence experiments, sections were co-incubated, overnight with two primary antibodies against GABA, GAD67, DARPP-32, CB, CR, NOS, or D1 raised in different species (mouse, monoclonal and rabbit, polyclonal). In one set of experiments sections were co-incubated with antibodies against GABA or GAD67 and CB, or NOS, or DARPP-32, in order to identify the distinct neurochemical identity of IM neurons. In another set of experiments sections were co-incubated with CB and NOS or DARPP-32 or CR, NOS with DARPP-32, and DARPP-32 with CR to identify potential overlap in the IM neuronal subpopulations. Finally, some sections were co-incubated with an antibody against D1 receptors and CB or NOS or DARPP-32, in order to detect potential receptor specificity or similarity among neurochemically distinct IM neurons. Buffer rinses were followed by incubation in fluorescent secondary antibodies (Alexa 488, Alexa 568, or Alexa 647; 1:200, in PBS, 0.1% BSA-C, 0.1% Triton-X, Molecular Probes, Eugene OR). Sections were mounted wet and coverslipped with ProLong Gold Antifade (Invitrogen, Grand Island, NY).

With the exception of the D1 receptor antibody that stained only the cytoplasm of labeled cells, all other antibodies stained the nucleus and cytoplasm. This was the case both for brightfield experiments stained with DAB and fluorescence experiments stained with Alexa fluorophores. Labeled neuronal profiles always had staining in the cytoplasm and in most cases dendritic or axonal processes were partially visible at high magnification.

Pre-embedding immunohistochemistry and processing for electron microscopy

Double and triple immunohistochemical methods were used to label NOS, CB and DARPP-32 in cases BI, BL and BN. Neurons were labeled either with silver-enhanced gold-conjugated secondary antibodies, DAB or tetramethylbenzidine (TMB), as described previously (Zikopoulos and Barbas, 2007; Medalla and Barbas, 2009; Timbie and Barbas, 2014, 2015). The three stains show distinct labeling at the EM: DAB appears as a dark uniform precipitate, silver-enhanced gold particles appear as circular clumps of variable size, and TMB as rod-shaped crystals. Sections were incubated overnight in the appropriate combination of primary antibodies raised in different species (mouse, monoclonal and rabbit, polyclonal: NOS, and/or CB, and/or DARPP-32, as described above). For triple-labeling experiments we used a combination of two mouse monoclonal primary antibodies for NOS and DARPP-32 and a rabbit polyclonal for CB, processed successively, using the Mouse-on-Mouse blocking kit (M.O.M. basic kit; Vector Laboratories) in between to prevent cross-reaction (Zikopoulos and Barbas, 2007; Medalla and Barbas, 2009; Timbie and Barbas, 2014, 2015). To preserve tissue integrity we used reduced concentration of Triton-X in all EM experiments (0.025%). To ensure adequate penetration of antibody reagents in the tissue we incubated tissue sections in a variable wattage microwave oven (8 min at 150 W in the Biowave; Ted Pella, Redding, CA, USA). Sections were then incubated overnight in the appropriate secondary gold-conjugated IgG (1:50, 1-nm gold particle diameter; GE Healthcare, Westborough MA) and in another secondary biotinylated antibody (anti-mouse IgG; 1:200, Vector) followed by AB-HRP.

The tissue was postfixed in 6% glutaraldehyde with 2% paraformaldehyde using a variable wattage microwave oven (3–6 min at 150 W in the Biowave; Ted Pella, Redding, CA, USA) until the fixative reached 30 °C, and then intensified with silver (6–12 min; IntenSE M kit; GE Healthcare) for labeling gold-conjugated antibodies. Sections were then processed for DAB followed by Avidin–Biotin block (AB block kit, Vector SP 2001). In the case of triple-labeling experiments, sections were then incubated with the appropriate third mouse secondary biotinylated antibody, followed by AB-HRP and processed for TMB and stabilized with DAB-cobalt chloride solution, as described (Zikopoulos and Barbas, 2007; Medalla and Barbas, 2009).

In control experiments, we omitted the primary antibodies to test the specificity of secondary antibodies, and used the AB blocking reagent prior to AB binding, or the M.O.M. kit prior to secondary antibody binding. In all control experiments there was no immunohistochemical labeling. In some experiments we reversed the order of precipitation methods and processed DAB staining before gold staining and silver enhancement. Distribution of labeling was overall similar with standard experiments (gold/silver first and then DAB), however, non-specific silver staining was elevated in the reverse experiments, because silver particles were attracted and bound with DAB precipitate.

Tissue sections were mounted on slides and quickly viewed under the light microscope, and images were captured with a CCD camera. Sections were then postfixed in 1% osmium tetroxide with 1.5% potassium ferrocyanide in PB, washed in PB and water, and dehydrated in an ascending series of alcohols (50–100%). While in 70% alcohol, blocks were stained for 30 min with 1% uranyl acetate (EM Sciences). Subsequently, they were infiltrated with propylene oxide and flat embedded in araldite at 60 °C. Small blocks of the IM neuropil with NOS, CB and DARPP-32 labeling were cut under a dissecting microscope from the araldite-embedded tissue and re-embedded in resin blocks. Serial ultrathin sections (50 nm) were cut with a diamond knife (Diatome USA, Hatfield, PA, USA) using an ultramicrotome (Ultracut, Leica, Wein, Austria) and collected on single slot pioloform-coated grids.

Data analysis and statistics

Unbiased stereology: light microscopy. We estimated the number and density of neurons and glial cells in IM in Nissl-stained sections ($n = 3$; cases AJ, AW, BO) and GABA-stained sections ($n = 1$; case BO) using the unbiased stereological method of the optical fractionator (Gundersen, 1986; Howard and Reed, 1998) with the aid of a commercial system (StereoInvestigator; MicroBrightField, Inc., Williston VT, USA), as described in previous studies (Barbas et al., 2005; Medalla and Barbas, 2006; Zikopoulos and Barbas, 2006; García-Cabezas and Barbas, 2014). We used cytoplasmic and nuclear features to distinguish neuronal and glial types, as described (García-Cabezas and Barbas, 2014). Briefly, we analyzed a minimum of five evenly spaced brain sections per case using systematic random sampling through IM. The stereological data included volume calculation for IM, which takes into consideration the sampled area and thickness of each section. We used as guard zones the top and bottom of each section (minimum 2 μm) and measured the actual mounted section thickness using the program software at each counting site. The counting frames (squares with sides in the range 50–70 μm; height = 5 μm) and grid spacing (squares with sides in the range 150–250 μm) were set to employ a fraction to yield a coefficient of error of < 10%, as recommended (Gundersen, 1986; Howard and Reed, 1998). For the sparse microglial cells, the coefficient of error was < 20%, as recommended for the monkey cerebral cortex (Peters et al., 2008). More than 300 cells were counted in each area analyzed per case. We additionally estimated the total number of GABAergic neurons in the amygdala, the relative proportion of IM inhibitory neurons in the amygdala, and the volume of the entire amygdala using the Cavalieri method.

Quantitative mapping: fluorescence microscopy and confocal imaging. We used fluorescence microscopy and confocal imaging to estimate the relative proportions and overlap of CB, NOS, and DARPP-32 IM neurons, through cell profile counts at sites chosen using a systematic, uniform random selection method (sampling fraction per section 1:5; cases BK, BR were used for overlap studies) and comparing with stereological estimates of the numbers and density of all Nissl- and GABA-stained IM neurons. To image fluorescent signal we used a Revolution dual spinning disk (DSD) white light confocal microscopy system (Andor, Belfast, UK). The DSD system is composed of a white light source (AMH-200-F6S) and a Clara Interline CCD camera attached to an Olympus BX63 microscope with a motorized reflected fluorescence system (model BX3-RFAA) and a motorized stage (model V31XYZE, Prior Scientific, Rockland, MA), controlled by an Olympus BX3-CBH U-MCZ controller box. Stacks of images were captured using a 40× objective (×400 magnification) or a 60× oil immersion objective (×600 magnification; Olympus), with MetaMorph NX software on a Dell Precision T3520 Workstation running Microsoft Windows 7 (32 bit). Filters specific to the wavelength of the distinct fluorophores were used to image separate channels which were captured individually and compiled into composite stacks using Fiji (Schindelin et al., 2012). Stacks were captured at 0.3–0.5-μm z-intervals in the IM neuropil.

3D reconstruction of neuronal populations in IM. To map and plot the distribution of neurochemically distinct IM neuronal subtypes we used exhaustive sampling in a series of sections (10–16 sections; distance between sections: 400–500 μm) from one additional case per marker (CB, NADPHd, DARPP-32, GABA). We outlined brain sections, placed architectonic borders of amygdalar nuclei, and mapped labeled neurons in each case with the aid of a commercial computerized microscope system and motorized stage (Neurolucida; MicroBrightField Inc.). The procedure involves setting a

reference point for every brain hemisphere analyzed, and as a result the outlines within a series are automatically registered and aligned to the actual corresponding sections, retaining information about the 3D coordinates of every mark or trace. To compare the topography and distribution of labeled neurons across series or cases and exhibit their overlap in IM, we compared sections from adjacent levels in the amygdala and reconstructed in three dimensions the entire nucleus using the free, open source software Reconstruct (Fiala, 2005), as described previously (Zikopoulos and Barbas, 2006, 2012). Briefly, we imported the outlines containing 3D information about the topography of labeling from each case in Reconstruct and co-registered and aligned them to generate 3D models. As a result, all markers and traces were registered stereotaxically and superimposed on the 3D models. Plots of labeled neurons in IM were exported and compiled into appropriate figures in Adobe Illustrator (Adobe Systems Inc., San José, CA, USA).

3D serial electron microscopy. Serial sectioning of blocks containing IM neuropil produced mini or long series (10–100 sections) that were analyzed using systematic random sampling to image labeled and unlabeled axon terminal profiles and their targets. We followed each bouton and associated postsynaptic targets throughout adjacent serial sections for each synapse and marked profiles as labeled only if clear labeling was present in more than three sections within the series. Background with appearance of non-specific gold staining in our material was overall low, partially because we omitted lead aspartate staining in the protocols. However, because silver-enhanced gold labeling of antigens can produce variable levels of background we used several additional approaches to reliably identify labeled structures, as described previously (Muly et al., 2009; Medalla and Barbas, 2012; Timbie and Barbas, 2014). We avoided sampling from the top and bottom 1 μm of each block, where background tends to be high. We also set a background threshold for each piece of tissue by estimating the size of silver-enhanced gold particles in mitochondria. This was the typical location of non-specific labeling in our experiments, where the size of each particle was less than 15 nm in diameter. Therefore, the size threshold for gold-positive elements was set to diameters larger than 15 nm. We also counted the number of non-specific silver-enhanced gold particles in mitochondria in several series from each experiment, and divided this value by the total volume of mitochondria in that series. Finally, we counted the total number of particles less than the size threshold in one out of every five sections of each series and expressed the background level as the estimated total volume of small particles (number of particles × spherical volume of a single particle 15 nm in diameter) per volume of tissue sampled. Using these estimates we set a stringent threshold for gold-positive elements to five times the density of gold in mitochondria or in other series elements. The relative distribution of specific gold labeling and the relative proportion of non-specific staining remained consistently low in our material, irrespective of possible differences between cases due to potential variation in tissue fixation that may affect antibody penetration and staining.

Images were imported in Reconstruct to mark synapses by type. We used classical criteria to identify synapses and their types as well as other profiles (Peters et al., 1991; Peters and Palay, 1996). Synapses are characterized by the aggregation of synaptic vesicles in the presynaptic bouton, the rigid apposition of the presynaptic and postsynaptic membranes, widening of the extracellular space and the presence of pre- and postsynaptic membrane specializations. Asymmetric synapses (type I) have thickened postsynaptic densities and rounded vesicles; symmetric (type II) synapses have thin postsynaptic densities and pleomorphic vesicles. Dendrites can be spiny, in which case the vast majority of synapses target the spines, or can be smooth or sparsely spiny and receive synapses mostly on their dendritic shafts. Axon terminals are >0.1 μm in diameter and contain synaptic vesicles and often have mitochondria. Dendritic shafts contain mitochondria, microtubules, and/or rough endoplasmic reticulum, while dendritic spines lack these organelles but may have a membranous sack-like spine apparatus.

Photography

We captured images of labeled cells in the IM at the optical microscope using a CCD camera (Olympus DP70) attached to a microscope (Olympus optical microscope, BX 60) connected to a personal computer using a commercial imaging system (DP-Controller). We captured labeled neuron profiles in the EM using a digital camera (ES1000W, Gatan, Pleasanton, CA, USA) at a magnification of 10,000–50,000×. Images were imported into Adobe Illustrator CS5 software (Adobe Systems Inc., San José, CA, USA) to assemble in figures. Fluorescent images were deconvolved using AutoDeblur (Media Cybernetics, Rockville, MD, USA) or Deconvolution Lab plugin for ImageJ. Minor adjustment of overall brightness and contrast were made but images were not retouched.

RESULTS

Topography and distribution

Inhibitory IM neurons were not confined to isolated cell clusters, as the commonly used name intercalated masses or clusters implies, but instead formed a continuous neuronal net that separates the lateral/basal and to a lesser extent the cortical nuclei from the dorsally located anterior, central, and medial amygdalar nuclei. In addition, IM neurons and their processes also separated the three nuclei of the basal division of the amygdala (BL, BM, La; Fig. 1). The continuity of this inhibitory net was particularly evident in three-dimensional reconstructions of plotted cells stained with Nissl or markers of GABAergic neurons from series of consecutive coronal sections through the rhesus monkey amygdala (Fig. 2). The GABAergic intercalated neurons were found in the spaces between the borders

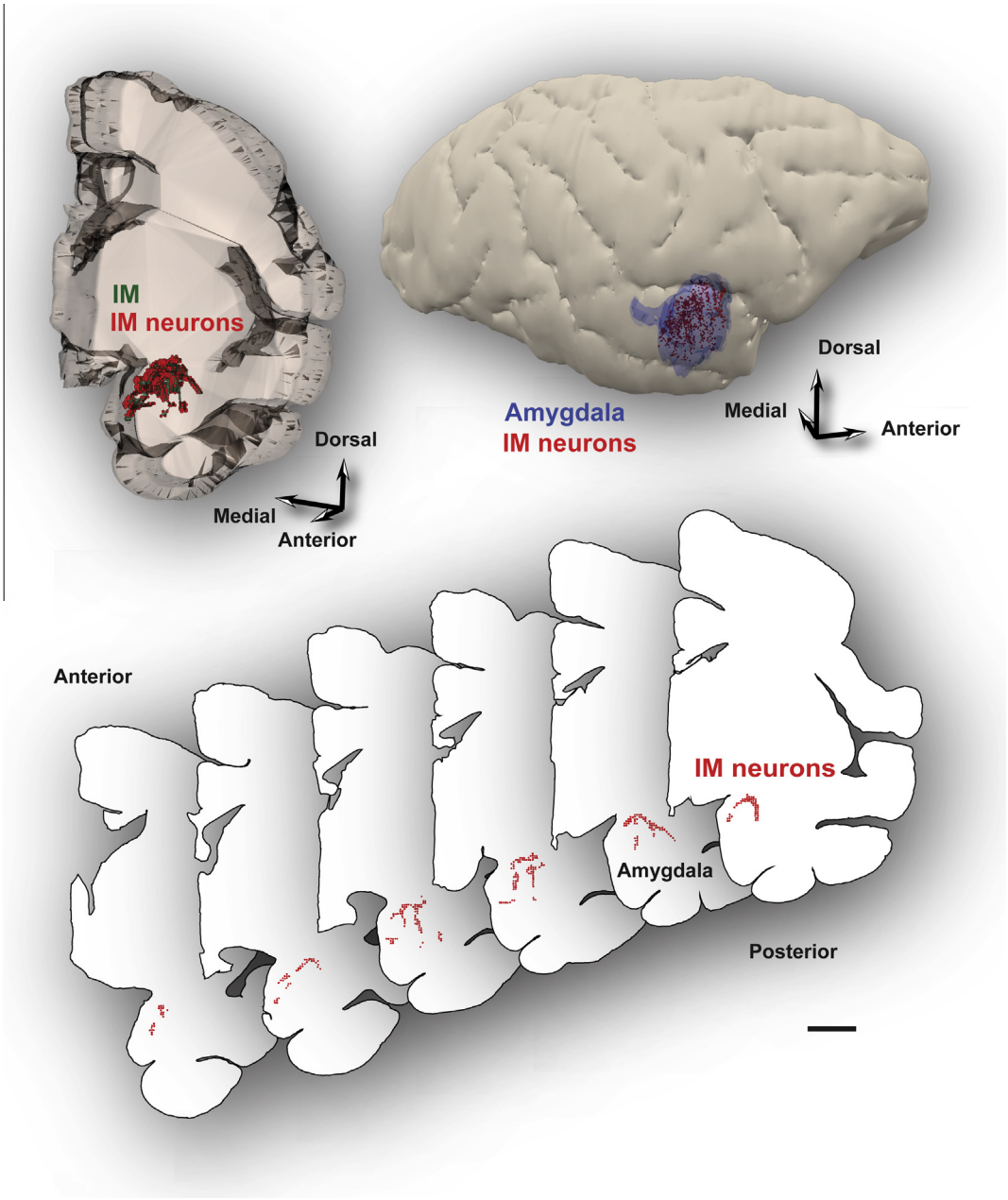

Fig. 2. GABAergic IM neurons form a continuous inhibitory net. IM neurons surround primarily the basal and lateral nuclei, and to a lesser extent, the cortical nuclei of the amygdala. *Top*, Reconstruction of the amygdala in the rhesus monkey in 3D shows the distribution of IM neurons (red dots) in tissue slab (left). The relative antero-posterior position of the amygdala is depicted on the lateral view of the right hemisphere (right). *Bottom*, Serial coronal sections were outlined and used to reconstruct the IM in 3D and map neurons in each case. Each red dot represents one plotted neuron. Note that IM neurons partly outline the basal nuclei. Scale bars = 5 mm. (For interpretation of the references to colour in this figure legend, the reader is referred to the web version of this article.)

of the basal, lateral, cortical, central, medial, and anterior amygdalar nuclei, within sites of fiber bundles that course through the amygdala (Fig. 3). Some IM neurons were also found along the borders of the amygdala with the external capsule and the caudate-putamen. Unlike the IM in rodents, which is prominent in the rostral half of the amygdala (Millhouse, 1986), the primate IM appeared to stretch throughout the antero-posterior axis of the amygdala. This is in line with the overall rotation of the amygdala around Ce in primates, likely due to the expansion of neighboring cortical areas.

Density and overall number of neurons in IM. We used stereology for unbiased estimate of the number and density of IM neurons from Nissl-stained tissue sections (three cases). To control for possible variability due to differential tissue shrinkage we independently estimated the volume of the entire amygdala in a total of six cases (including the three cases used for the Nissl counts), using the Cavalieri method, and found no differences (deviation among cases = 2%; amygdala volume ± SEM = 195 ± 4 mm^3). Our findings were within the range reported in other studies (Emery et al., 2001;

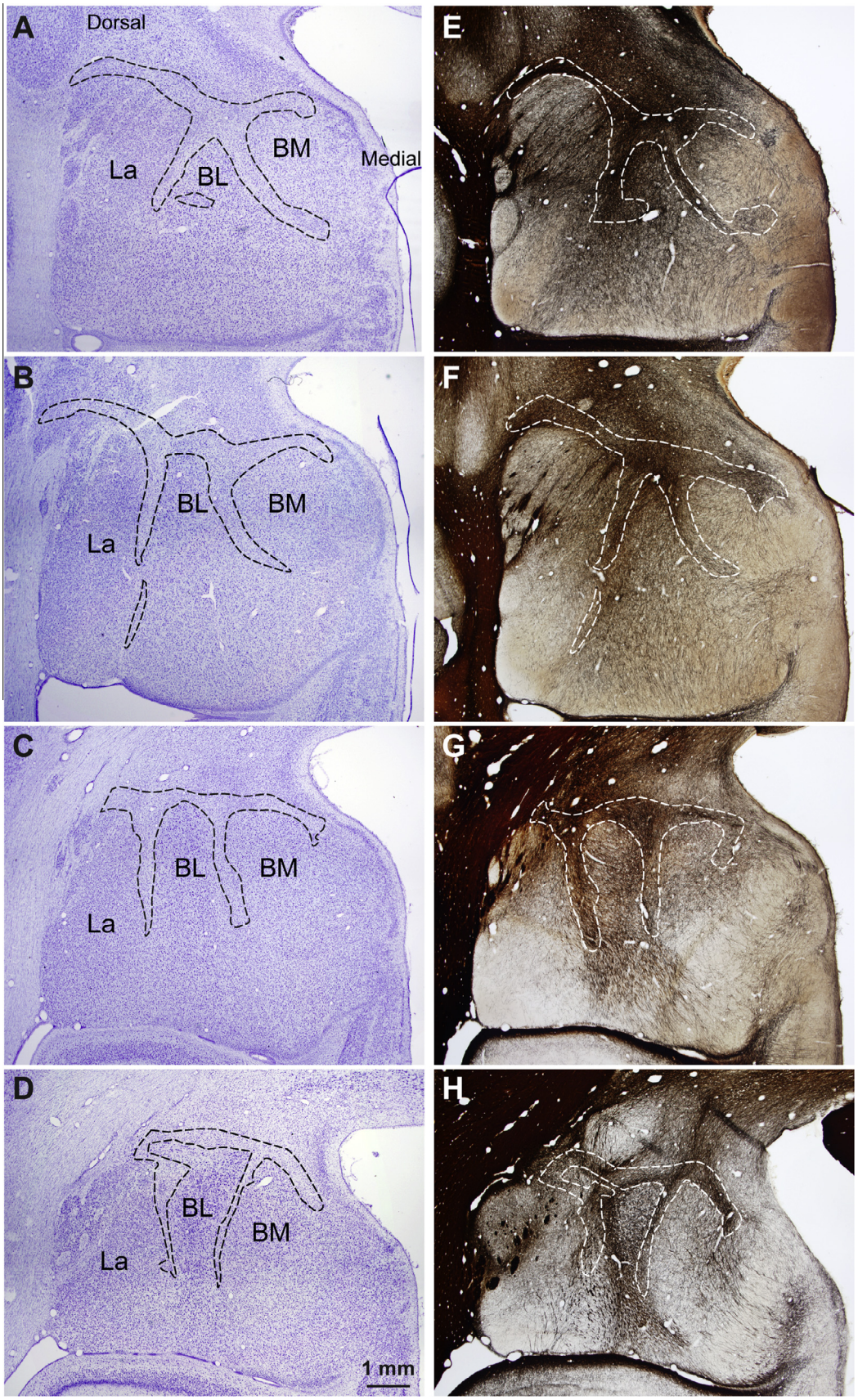

Fig. 3. The IM of the rhesus macaque in serial coronal sections through the amygdala. (A–D) Nissl-stained sections from anterior (A) to posterior (D) levels of the amygdala. (E–H) Matched sections stained for myelin. Dotted outlines indicate approximate borders of IM neuropil in a region rich in glia and myelinated fiber tracts that contain mostly small neurons positioned between the main amygdalar nuclei. Scale bar in D applies to all panels.

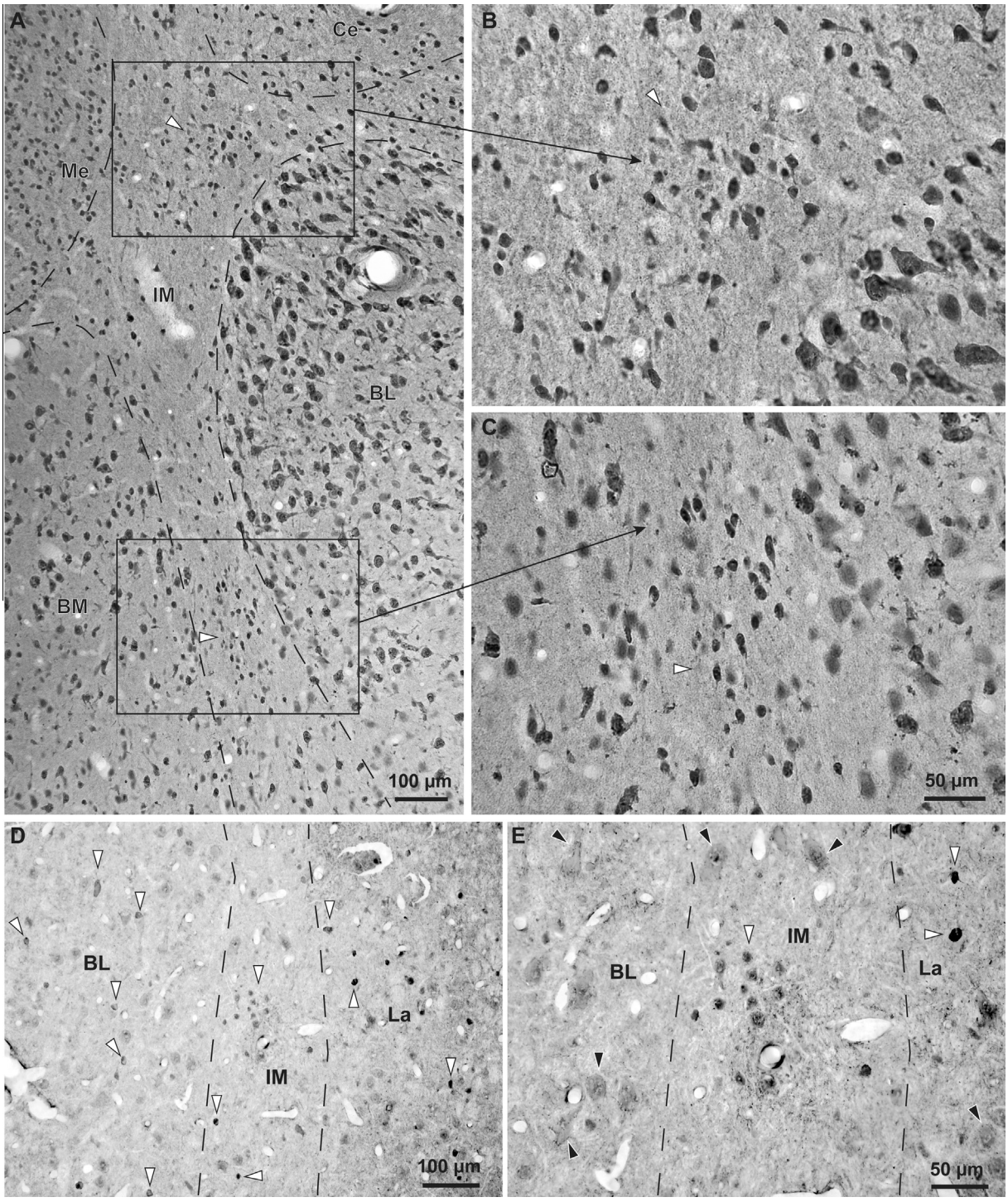

Fig. 4. The IM clusters in the rhesus monkey brain. NeuN and GABA immunohistochemistry in the IM of the rhesus monkey amygdala. (A–C) Coronal brain section stained for NeuN through the amygdala. (A) Low magnification shows the demarcated IM, including some clusters (white and black, silhouette arrowheads). (B–C) IM clusters are seen at higher magnification. Note the small size of IM neurons compared to neurons in BL and BM. (D and E) Isolated inhibitory neurons and small IM neuron clusters (white and black, silhouette arrowheads) are labeled with GABA. BL and La also contain inhibitory GABAergic neurons that can be darkly or lightly stained (white and black, silhouette arrowheads). In contrast, pyramidal neurons in BL and La are larger in size, often have pyramidal shape, and have very light, background levels of staining in their cytoplasm (black arrowheads in E). In most cases pyramidal neuron somata appear to be surrounded by darkly-stained GABAergic axon terminals that form perineuronal complex basket formations, previously described on pyramidal neurons in cortical and amygdalar areas of many species, including monkeys and humans (black arrowheads in E). Scale bar in C applies to B and C.

Chareyron et al., 2011), suggesting that tissue shrinkage was similar among the cases analyzed. Neurons were identified by the presence of stained cytoplasm around the entire perimeter of the nucleus. Large neurons had a large and distinct nucleolus. Small neurons had a less defined nucleolus and several clumps of heterochromatin

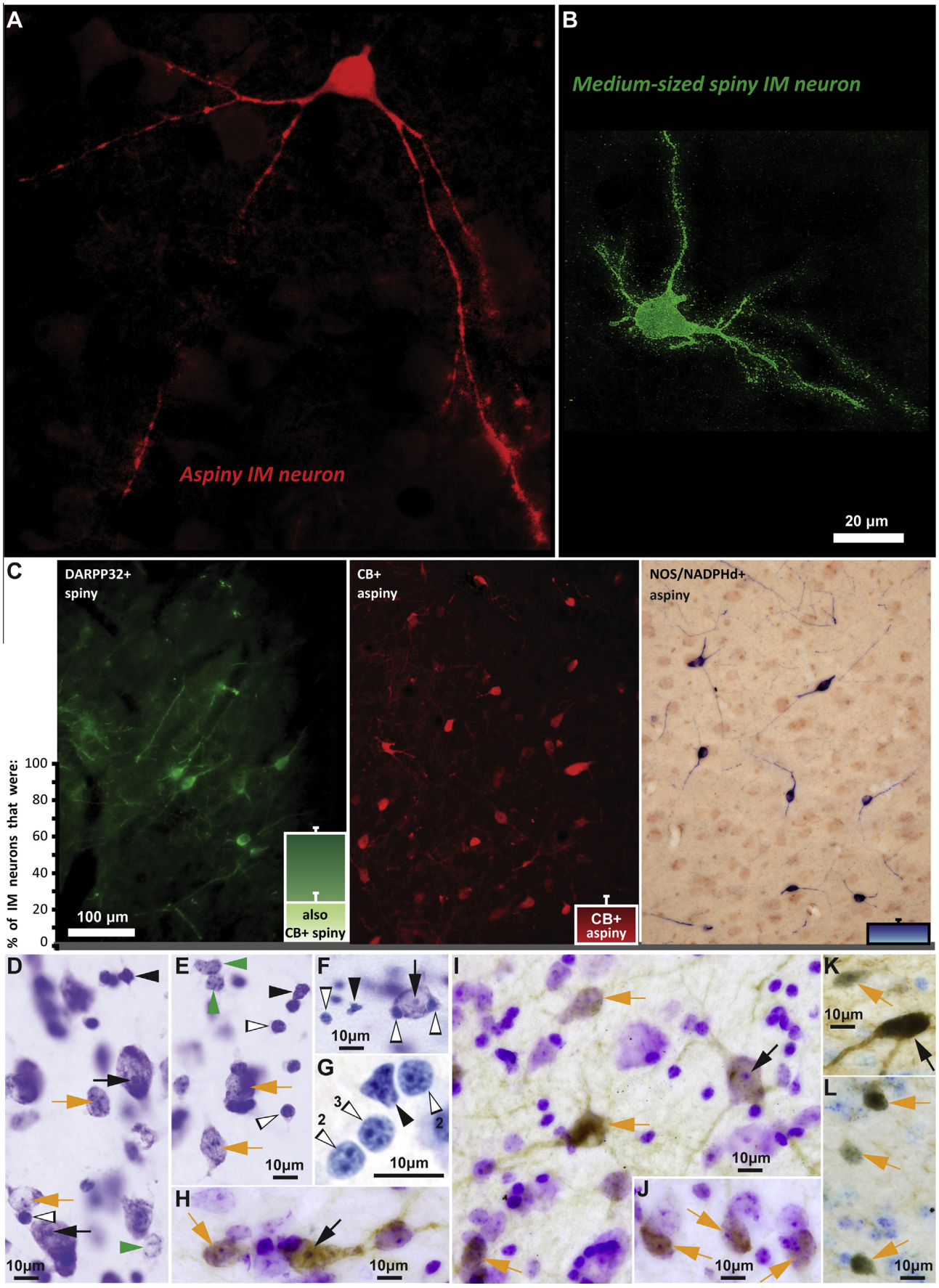
A
Aspiny IM neuron
B
Medium-sized spiny IM neuron
20 μm
C
DARPP32+
spiny
100 μm
also
CB+ spiny
CB+
aspiny
CB+
aspiny
NOS/NADPHd+
aspiny
% of IM neurons that were:
100
80
60
40
20
0
D
10μm
E
10μm
F
10μm
G
3
2
2
10μm
H
10μm
I
10μm
J
10μm
K
10μm
L
10μm

around the nucleolus, in the nucleoplasm and under the nuclear envelope (García-Cabezas and Barbas, 2014). There were about 445,000 IM neurons in each brain hemisphere (mean number ± SEM: 444,925 ± 92,439), occupying a volume of 18 ± 2 mm^3, with an average density of 24,895 ± 2,605 neurons/mm^3. The distribution of neurons was anisotropic, with the highest density found in the dorsal strip that separates the basal and lateral from the central nuclei, and two clusters situated between the basal and lateral nuclei (Fig. 4). The density in these densely packed IM clusters was almost three times higher (69,896 neurons/mm^3). The localized increase in neuron density of these particular IM segments, gave an overall appearance of cell clumps interconnected with thin neuronal sheets that were more sparsely populated.

The stereological neuron count was also assessed using an antibody against GABA (1 case). The number of GABA-labeled neurons in IM was 473,963 with a density of 21,159 neurons/mm^3, in line with the Nissl estimates. Inhibitory IM neurons constituted approximately 17% of all inhibitory neurons in the amygdala.

Density and distribution of glia in IM. We distinguished types of glial cells (Fig. 5D–G), as described previously (García-Cabezas and Barbas, 2014), based on classical descriptions (Ramón y Cajal, 1896, 1899/2002, 1913; del Río-Hortega, 1919, 1921, 1928, 1932) and more recent work (Ling et al., 1973; O'Kusky and Colonnier, 1982; Gabbott and Stewart, 1987). Briefly, astrocytes had round or oval nuclei, homogeneous nucleoplasm and several rounded clumps of heterochromatin, some of which were located under the slightly irregular nuclear membrane (Fig. 5D, E, green arrowheads). The cytoplasm of astrocytes was not stained with Nissl but in rare occasions we observed pigmented granular inclusions close to the nucleus. Oligodendrocytes had round and darkly stained nuclei, which were usually smaller than the nuclei of astrocytes, with a smooth nuclear membrane and a few clumps of heterochromatin (Fig. 5D–G, silhouette arrowheads). Microglia had darkly stained, elongated or polylobular nuclei without visible heterochromatin and cytoplasm; in some cases we observed cytoplasmic granular inclusions close to the nuclear lobules (Fig. 5D–G, black arrowheads). The different types of glial cells were also readily recognizable in the EM (Peters et al., 1991).

There were about two times as many glial cells as neurons in IM, most of which were oligodendrocytes (mean density ± SEM: 28,296 ± 6,161), followed by astrocytes (mean density ± SEM: 19,989 ± 2,977) and microglia (mean density ± SEM: 4,497 ± 792). This pattern of distribution is typical in areas between nuclei that are rich in fiber bundles (Fig. 3).

Cytology and neurochemistry

Division of IM neurons by dendritic spiny or smooth morphology. There were two types of intercalated neurons: spiny and aspiny (Fig. 5A–C). Spiny neurons were the most abundant (mean ± SEM: 63 ± 3%) and had small- or medium-sized somata (mean diameter ± SEM: 13 ± 0.2 μm; diameter range: 7–22 μm). Depending on their location, the cell bodies were round or elongated, and the dendritic trees were round or bipolar. Accordingly, IM neurons located in the narrow corridors between the basal and lateral amygdalar nuclei were more often elongated and bipolar than not, whereas IM neurons located in the larger space under CE were often round and multipolar. The vast majority of the spiny neurons resembled the striatal medium-sized spiny neurons; they had 2–4 primary dendrites enriched with spines. In Nissl-stained sections the nucleus of these neurons appeared round with clumps of darkly stained heterochromatin along the nuclear membrane and the cytoplasm was very thin and lightly stained (Fig. 5D–L, orange arrows). Very few of these neurons were large, defined as those exceeding 20 μm in diameter. Large cell bodies were more common among the aspiny neurons (~37%), which were on average slightly larger (mean diameter ± SEM: 16 ± 0.4 μm; diameter range: 10–25 μm) and had varicose dendrites. The nuclei of these neurons appeared round or elongated and in most cases contained one clearly defined nucleolus (Fig. 5D–F, H, I, K, black arrows). Large IM neurons did not exceed 5% of the total neuronal population and were distributed throughout the IM. In contrast, small- and medium-sized IM neurons often formed discrete densely packed clusters.

Fig. 5. Distinct morphological and neurochemical subtypes of inhibitory IM neurons. (A and B) Morphologically-distinct aspiny (red, stained with CB) and spiny (green, stained with DARPP-32) IM neurons. (C) The three distinct neurochemical subtypes of IM neurons and their relative proportion in the rhesus monkey IM. Note that all spiny neurons in IM were DARPP-32+ and about a third of them were also CB+. Aspiny IM neurons belonged to two classes: those that were CB+ and those that were NOS/NADPHd+. The IM neuron breakdown shown in the bar plots (N = 4) was as follows (mean ± SEM): 63 ± 3% (spiny DARPP-32; a third of these spiny DARPP-32+ neurons also co-expressed CB) + 23 ± 7% (aspiny CB+) + 14 ± 2% (aspiny NOS+). (D–G) Nissl-stained neurons and glia in IM. (H–L) Nissl-counterstained neurons in IM, also labeled for DARPP-32 (H–J), NOS (K), and CB (L), shown as brown DAB precipitate. Different arrows in D–L indicate all identified cell types, based on the size of their cell body, the presence or paucity of stained cytoplasm, size of nucleus, and the presence of one clearly defined nucleolus or multiple heterochromatin clumps, as follows: Black arrows: Large/medium neurons with one clearly defined nucleolus; Orange arrows: Small neurons with multiple heterochromatin clumps; Green arrowheads: Astrocytes, no visible cytoplasm and multiple heterochromatin clumps; Black arrowheads: Microglia, no visible cytoplasm, darkly stained and irregularly-shaped nucleus; White and black, silhouette arrowheads: Oligodendrocytes, no visible cytoplasm, darkly stained and oval or round-shaped nucleus with one to four thick heterochromatin clumps situated under the nuclear envelope (note number of heterochromatin clumps in panel G with lightly stained glial cells, resembling overexposure and high dynamic range during live imaging). Scale bar in B applies to A and B. (For interpretation of the references to colour in this figure legend, the reader is referred to the web version of this article.)

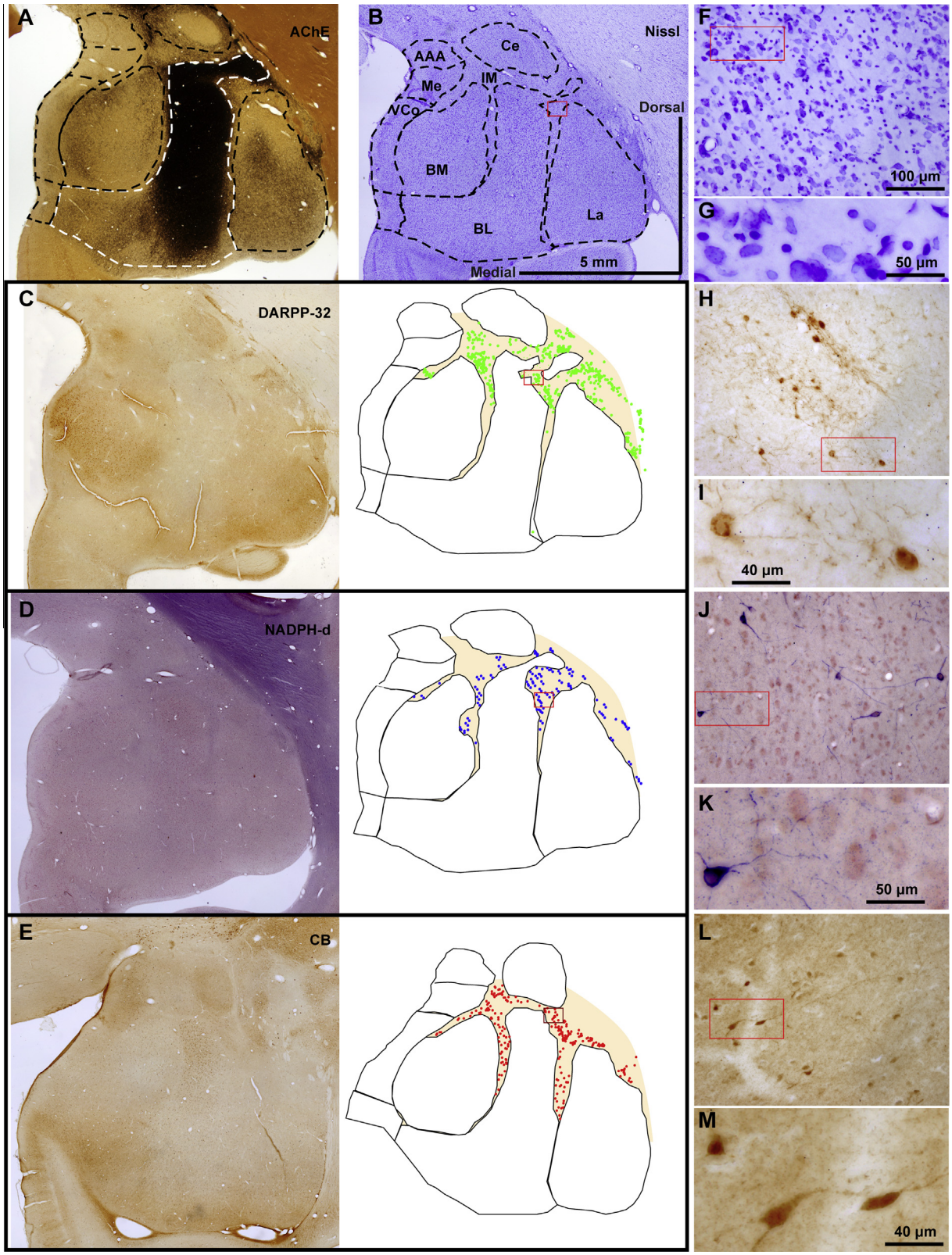

Fig. 6. Intermingling of different types of inhibitory IM neurons in the rhesus monkey amygdala. (A–E) Low power view of the amygdala in matched coronal sections show architectonic features and the outlines of amygdalar nuclei (obtained from A and B), and plots of distinct morphological and neurochemical IM neuron subtypes. (A) section stained for AChE; (B) section stained with Nissl; (C) section stained with DARPP-32; (D) section stained with NADPHd; (E) section stained with CB. (F–M) Progressively higher power views of red rectangular insets in B-E and F, H, J, L show labeled IM neurons. Most DARPP-32+ neurons and some CB+ neurons form neuronal clusters however, most CB+ and all NADPHd+ neurons are loosely distributed within the IM neuropil and in some cases appear to surround the clusters. Scale bar in B applies to A–E; Scale bar in F applies to F, H, J, L. (For interpretation of the references to colour in this figure legend, the reader is referred to the web version of this article.)

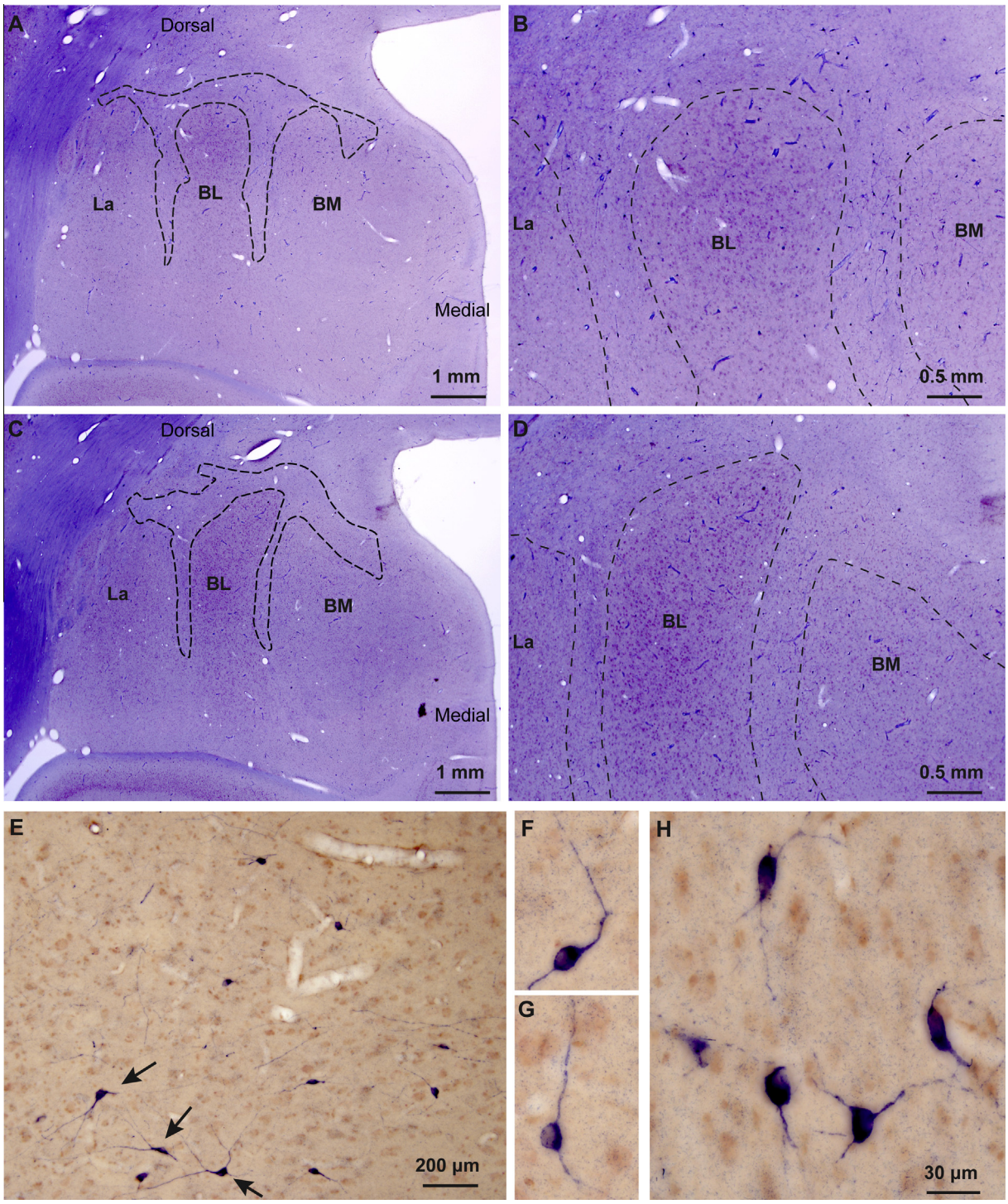

Fig. 7. NADPHd in the IM of the rhesus monkey amygdala. (A–D) Low (A, C) and matching higher (B, D) magnification of the amygdala in serial coronal brain sections show cytoarchitectonic features and NADPHd label. Dotted outlines (A, C) indicate approximate borders of IM neuropil. This histochemical reaction labels neuronal processes in a Golgi-like manner, highlighting the increased density of NADPHd+ neurons and the continuity of labeled neurons and their processes in the IM neuropil. Counterstaining with neutral red contrasts the blue IM neuropil region between the main amygdalar nuclei, which is rich in glia, myelinated fiber tracts, and has a high density of NADPHd+ neurons and processes, against a darker, mostly purple/red region occupied by larger neurons in other nuclei. (E–H) High magnification shows small/medium (E–G) and large (E: black arrows, H) NADPHd+ neurons and their processes in IM. Scale bar in H applies to F–H. (For interpretation of the references to colour in this figure legend, the reader is referred to the web version of this article.)

Division of IM neurons into three distinct neurochemical classes. There were three non-overlapping neurochemical populations of IM neurons, in descending order of abundance (Fig. 5C, bars, N = 4): (1) Spiny DARPP-32+ neurons were the most numerous (mean ± SEM: 63 ± 3%). A third of them

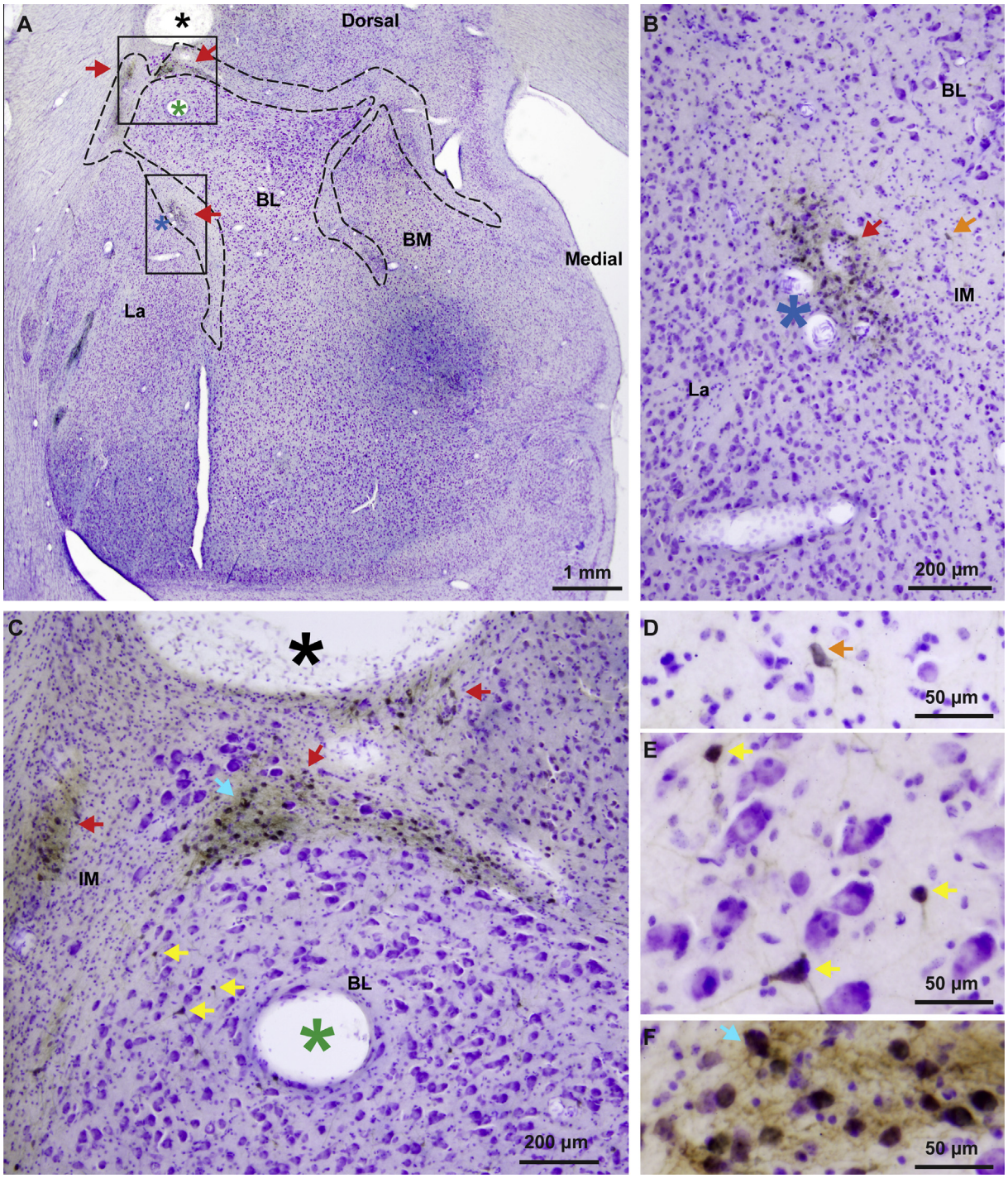

Fig. 8. IM clusters in the rhesus monkey amygdala contain mostly small/medium DARPP-32+ neurons. (A–F) Increasing magnifications of a coronal section of the amygdala immunolabeled for DARPP-32 (brown DAB precipitate) and counterstained with Nissl to show cytoarchitectonic features. Dotted outline in A shows approximate borders of the IM neuropil. Rectangles in A are magnified in B and C. Asterisks indicate position of matching blood vessels. Red arrows point to IM neuron clusters, shown at higher magnifications in B and C; yellow and orange arrows point to some DARPP-32+ neurons seen outside the clusters within the IM neuropil and are shown at higher magnification in D and E. The blue arrow in C points to a cluster of IM neurons that is magnified in F. The continuity of the IM neuropil is highlighted by a light and dark brown label, due to staining of DARPP-32+ neurons and their processes within IM. (For interpretation of the references to colour in this figure legend, the reader is referred to the web version of this article.)

co-expressed the calcium-binding protein CB (Fig. 5C, bar) and a few co-expressed CR. Most of these neurons were small or medium-sized and very few were large; (2) Aspiny neurons that expressed the calcium-binding protein CB and in some cases co-expressed CR (mean ± SEM: 23 ± 7%); and (3) Aspiny neurons that expressed NOS or NADPHd (mean ± SEM: 14 ± 2%). Some NOS + neurons were among the largest IM

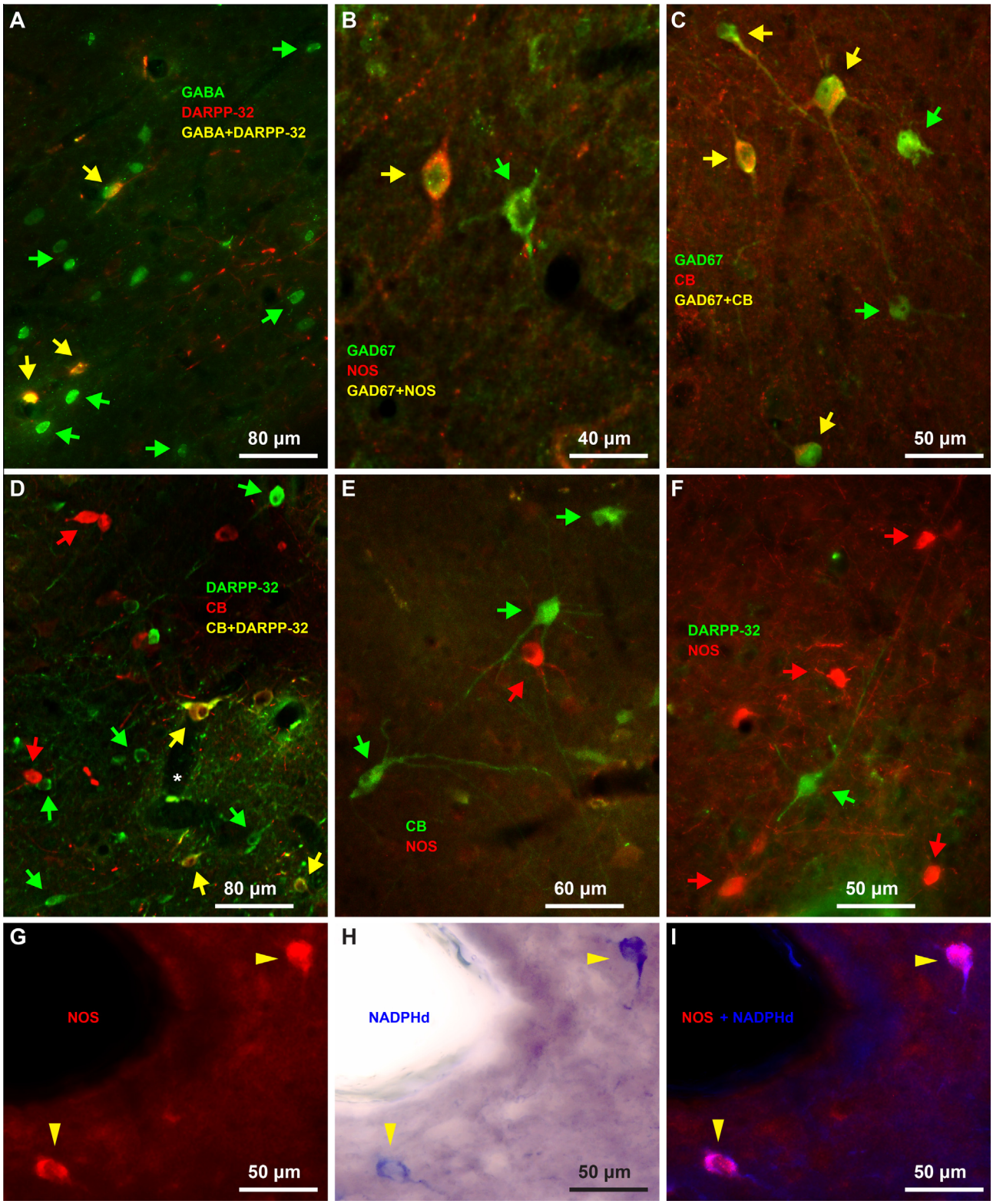

Fig. 9. Biochemical features of IM inhibitory neurons. (A) All DARPP-32 neurons co-localize with GABA (yellow arrows). (B and C) NOS neurons (B) and CB neurons (C) also express the inhibitory marker GAD67 (yellow arrows). (D) Some IM neurons express DARPP-32 and calbindin (yellow arrows). (E) CB expressing neurons (green arrows) do not overlap with NOS neurons (red arrows). (F) DARPP-32 expressing neurons (green arrows) do not overlap with NOS neurons (red arrows). (G–I) NOS and NADPHd co-localize in the same neurons (yellow arrowheads). The distinct neurochemical types of IM neurons are largely intermingled, however, in some cases (D, F) aspiny IM neurons appear to surround spiny IM neurons. Green and red arrows show some single-labeled neurons in panels (A–F). (For interpretation of the references to colour in this figure legend, the reader is referred to the web version of this article.)

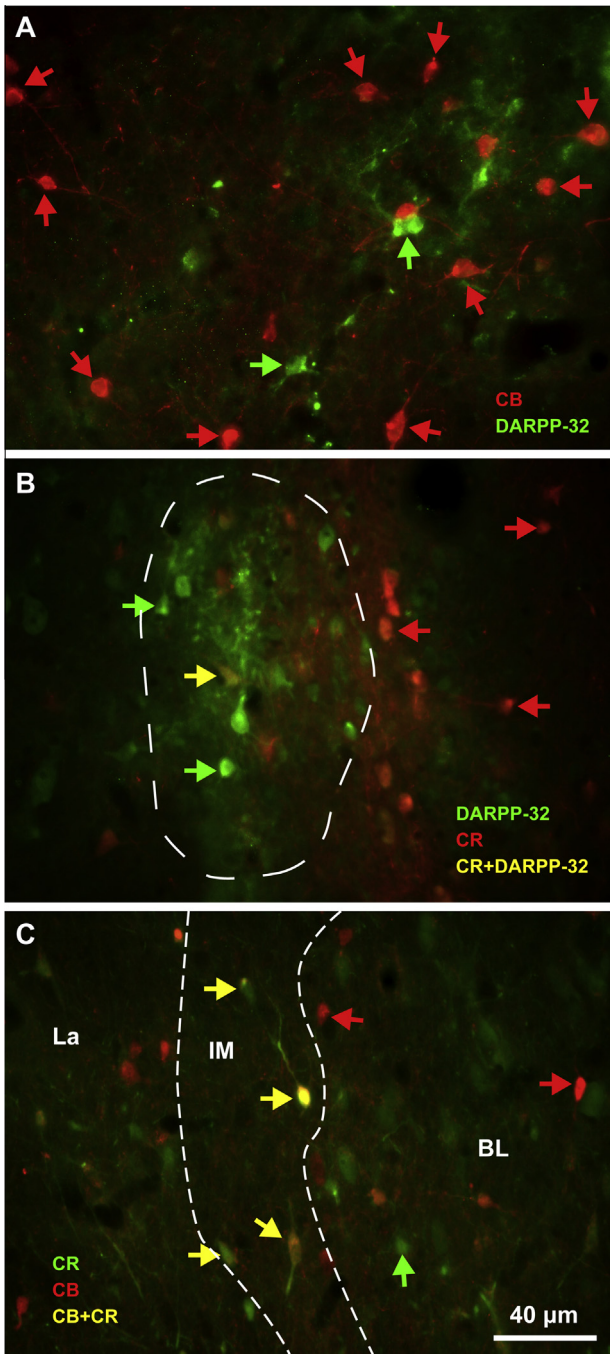

Fig. 10. Biochemical features of IM inhibitory neurons. (A) Aspiny CB+ IM neurons (red arrows) appeared to surround DARPP-32+ IM neurons (green arrows) at IM levels where there was no or little co-localization of these markers. (B) CR+ IM neurons (red arrows) were typically outside clusters of DARPP-32+ IM neurons (green arrows) at IM levels where there was little co-localization of these markers (one double-labeled cell marked with a yellow arrow). (C) Occasionally, CR (green arrows) and CB (red arrows) co-localized in the same IM neurons (yellow arrows). White dotted lines delineate IM neuropil. Scale bar in C applies to all panels. (For interpretation of the references to colour in this figure legend, the reader is referred to the web version of this article.)

neurons, exceeding 20 μm in diameter (Figs. 5C, 6J, K and 7E–H). Interestingly, the three neurochemically distinct types of IM neurons were intermingled and present throughout the antero-posterior and medio-lateral extent of IM (Fig. 6). However, small/medium-sized DARPP-32+ IM neurons were often clustered in densely packed groups (Figs. 6C, H and 8), although some appeared isolated, in agreement with previous studies in rhesus monkeys (Barbas et al., 1993). Most CB+ and all NOS+ IM neurons were not packed in clusters but were widely distributed within the IM neuropil and in some cases were positioned around clusters. CR did not label a distinct IM neuron subpopulation, along the spiny vs aspiny, or large vs small neuron groups, as the other three markers (DARPP-32, CB, and NOS), and was not expressed by all CB neurons in IM. There were no PV+ neurons in the rhesus monkey IM. Figs. 9 and 10 show examples of multiple labeling of the distinct neurochemical classes of inhibitory neurons in IM.

All IM neurons were GABAergic and expressed D1 dopaminergic receptors (Figs. 4D, E, 9A–C and 11). Staining with GABA or NeuN labeled the cell body and nucleus of IM neurons (Fig. 4). All amygdalar nuclei contained inhibitory GABAergic neurons that were darkly or lightly stained. In contrast, pyramidal neurons in BL, BM and La had very light, background levels of staining in their cytoplasm, often had pyramidal shape and were larger in size. In most cases pyramidal neuron somata were surrounded by darkly stained GABAergic axon terminals that formed perineuronal complex basket formations. These formations were previously seen on pyramidal neurons in cortical and amygdalar areas of many species, including monkeys (McDonald and Augustine, 1993) and humans (Marin-Padilla, 1970; Blazquez-Llorca et al., 2010). The D1 receptor antibody stained only the cytoplasm of neurons proximally, giving them a speckled appearance (Fig. 11). Other histochemical and immunohistochemical labeling of IM neurons additionally produced moderate to strong staining of their dendritic trees, mostly confined within the regions between other amygdalar nuclei, in areas we designated as IM neuropil (Figs. 3, 4 and 6–8).

Synaptic features and interconnectivity within the IM neuropil

We conducted quantitative analysis of synapses in the IM neuropil at very high resolution in the EM after immunohistochemical labeling against DARPP-32, CB, or NOS (Fig. 12). This analysis showed that most presynaptic axon terminals that formed synapses on labeled IM neurons were unlabeled (~90%), and most were asymmetric and presumed to be excitatory (~80%). The presynaptic axon terminals forming these asymmetric synapses were unlabeled and contained round vesicles. The post-synaptic sites were labeled spines or dendrites of IM neurons with a dense post-synaptic density (PSD), characteristic of asymmetric, excitatory synapses. The rest of the synapses on labeled IM neurons were symmetric (~20%) and presumed to be inhibitory. The pre-synaptic axon terminals in these synapses contained pleomorphic vesicles and the post-synaptic sites did not have a dense PSD. Interestingly, in our extensive sample of ~1000 synapses, where the post-synaptic site was labeled by one of the three markers (DARPP-32, NOS,

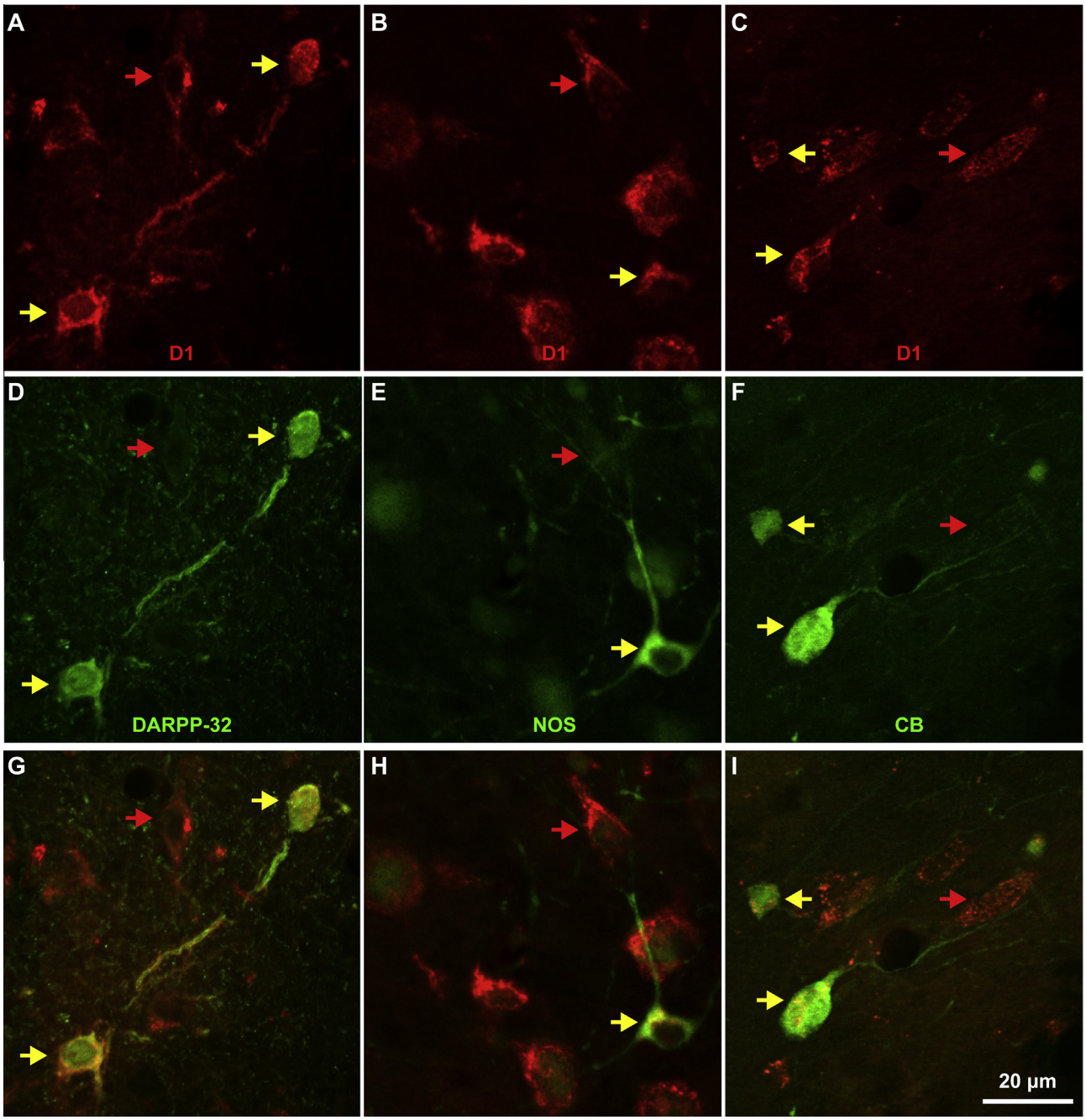

Fig. 11. All neurons of three distinct neurochemical subtypes of DARPP-32, NOS, or CB in IM express D1 receptors. (A–C) Three high magnification fields through the IM show D1 receptor expression in all neurons (red and yellow arrows). (D–F) In the same fields some neurons express DARPP-32, NOS, or CB (yellow arrows). (G–I) All neurons expressing one of the three distinct neurochemical subtypes of IM neurons express D1 (yellow arrows). Scale bar in I applies to all panels. (For interpretation of the references to colour in this figure legend, the reader is referred to the web version of this article.)

CB), we found that 10% of axon terminals were labeled and formed symmetric synapses only with aspiny CB+ and NOS+ IM neurons. We did not find labeled axon terminals forming symmetric synapses on IM neurons labeled with DARPP-32. When NOS+ IM neurons received symmetric synapses from labeled axon terminals they were either DARPP-32+ or NOS+. When CB+ IM neurons received symmetric synapses from labeled axon terminals they were either NOS+ or CB+ (Fig. 12).

DISCUSSION

We present novel evidence on the architecture of IM in the primate amygdala. Our quantitative study is the first to highlight important structural and histochemical features of inhibitory IM neurons and their specialized intrinsic circuits in primates, at multiple scales of analysis from the system to the synapse. Based on these findings we propose novel mechanisms for the filtering, integration and transmission of signals in the

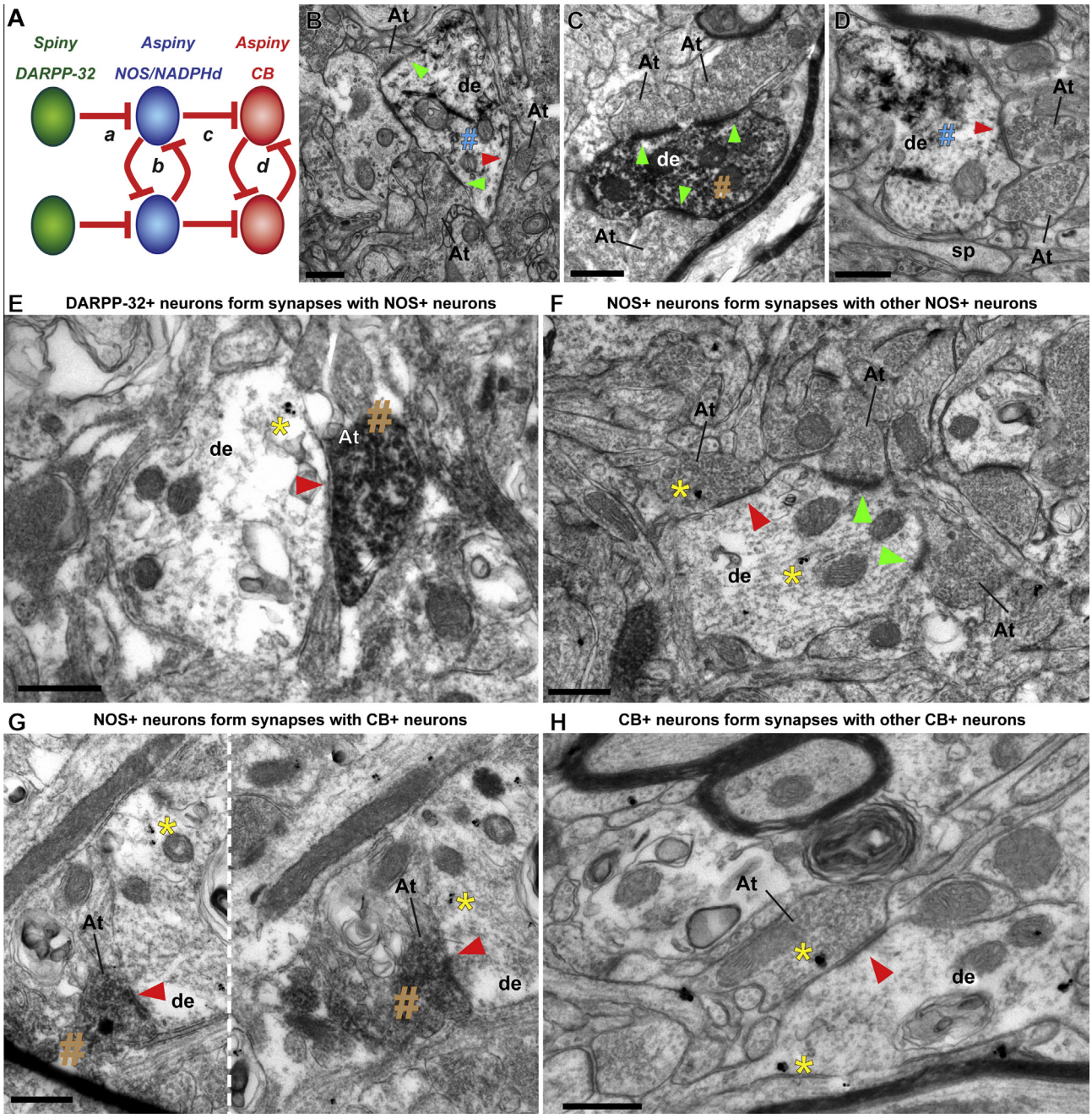

Fig. 12. Synapses in IM neuropil and local amygdalar circuitry in primates. (A) Plausible connectivity among IM cells in rhesus macaque, based on quantification of labeled symmetric, presumed inhibitory, synapses at the EM. Red lines connecting distinct neurochemical subtypes of IM neurons indicate inhibitory synapses. (B) Dendrite (de) of inhibitory IM neuron labeled with GABA (visualized with TMB, blue #) has two asymmetric (presumed excitatory, green arrowheads) and one symmetric (presumed inhibitory, red arrowhead) synapses with three unlabeled axon terminals (At). (C) Dendrite (de) of inhibitory IM neuron labeled with CB (visualized with DAB, brown #) has three asymmetric synapses (green arrowheads) with three unlabeled axon terminals (At). (D) Dendrite (de) of inhibitory IM neuron labeled with GAD67 (visualized with TMB, blue #) forming one symmetric synapse (red arrowhead) with an axon terminal (At). (E) DARPP-32+ neurons form synapses with NOS+ neurons in IM. Symmetric synapse (red arrowhead) between DARPP32+ axon terminal, labeled with DAB (brown #), and NOS+ dendrite, labeled with gold (yellow *), as illustrated in circuit "a" in (A). (F) NOS+ neurons form synapses with other NOS+ neurons in IM. Symmetric synapse (red arrowhead) between NOS+ axon terminal and NOS+ dendrite, labeled with gold, as illustrated in circuit "b" (A). Gold labeling is highlighted by a yellow *. Asymmetric synapses on the same dendrite from non-labeled axon terminals are shown with green arrowheads. (G) NOS+ neurons form synapses with CB+ neurons in IM. Series of adjacent EM photomicrographs, separated by a white dotted line, show symmetric synapse (red arrowheads) between NOS+ axon terminal, labeled with DAB (brown #) and CB+ dendrite, labeled by gold, as illustrated in circuit "c" (A). Gold labeling is highlighted by a yellow *. (H) CB+ neurons form synapses with other CB+ neurons in IM. Symmetric synapse (red arrowhead) between CB+ axon terminal and CB+ dendrite, labeled with gold, as illustrated in circuit "d" (A). In all images, At: axon terminal; de: dendrite; sp: spine; yellow *: gold labeling; blue #: TMB labeling; brown #: DAB labeling; red arrowhead: symmetric synapse (inhibitory); green arrowhead: asymmetric synapse (excitatory); Scale bar = 0.5 μm. (For interpretation of the references to colour in this figure legend, the reader is referred to the web version of this article.)

primate amygdala, consistent with the diverse roles of IM in processing stimuli associated with emotions and learning.

Defining the IM in primates

A basic organizational feature of the amygdala is its division into mostly excitatory, cortical-like, and inhibitory, striatal-like regions (De Olmos et al., 1985; De Olmos, 1990; Amaral et al., 1992; De Olmos and Heimer, 1999; Price, 2003; Sah et al., 2003; Waclaw et al., 2010; John et al., 2013), with different morphologic and physiologic properties (Mosher et al., 2010). Interposed between these two major regions are the inhibitory IM, which also infiltrate the narrow spaces that separate the nuclei of the basal complex in rhesus monkeys. The dendritic trees of IM neurons were largely confined within these inter-nuclear corridors, forming an extensive neuronal net positioned to intercept traffic. Contrary to the common reference of "clusters", IM neurons in macaques are organized into a continuum within the amygdala. The continuity of this inhibitory neuronal net could only be appreciated after immunohistochemical labeling for DARPP-32 and NADPHd or NOS that produced Golgi-like staining of neurons and their processes. The prominent clusters of small/medium sized neurons were continuous with more sparsely populated narrow corridors of neurons of various sizes. The IM complex was embedded within an extensive net of stained dendritic processes between the amygdalar nuclei, in agreement with previous studies of IM in rats and humans (Millhouse, 1986; Urban and Yilmazer-Hanke, 1999; Marcellino et al., 2012).

Our findings indicate that the small, densely packed clusters of IM neurons constitute only a minor part of the IM in the primate amygdala. In line with this assessment, a previous study in primates (Carlo et al., 2010), reported the volume and number of Nissl-stained neurons only in the densely- packed IM clusters of the rhesus monkey, which led to significantly lower estimates than in this study (IM volume: 0.38 mm^3 vs 18 mm^3; number of neurons: 25,600 vs 445,000). The magnitude of the differences in the estimates in the two studies suggests that not all IM clusters were included in the analyses in the Carlo et al., study, which was not focused on IM and did not include outlined maps of the analyzed clusters. The disparity in the estimated number of neurons in IM can also be partly explained by methodological differences between the two studies. For example, in the Carlo et al., study the authors counted only neurons with a nucleus that contained one clearly defined nucleolus. However, many neurons in IM have nuclei without a clear nucleolus, which have instead clumps of darkly stained heterochromatin along the nuclear membrane, nucleoplasm and around the nucleolus, features that are common in small neurons, in general (Ramón y Cajal, 1896, 1899/2002; García-Cabezas and Barbas, 2014). In addition, in the Carlo et al., study the authors defined the IM clusters following previous descriptions (Pitkanen and Amaral, 1991, 1994, 1998), which included only the most prominent dense clusters of small darkly Nissl-stained cells that are located between BL and BM, or between BL and La, below Ce, or at the ventromedial tip of BM. Following this demarcation of IM to include only small neurons confined to the well-delineated IM clusters in our cases, the neuronal densities in the two studies were similar [density: 69,896 neurons/mm^3 (this study) vs 67,368 neurons/mm^3 (Carlo et al., 2010)].

The small size of the cell bodies in the IM clusters and their dark Nissl staining had earlier misled investigators into thinking that they were clumps of glia, but later were shown to contain neurons [for a historical perspective see (Millhouse, 1986)]. There were twice as many glia as neurons within the IM neuropil, a ratio that was significantly higher than the average amygdala glia/neuron ratio of approximately 1.3 (Chareyron et al., 2011). This is not surprising, given the positioning of IM between the main amygdalar nuclei within fiber bundles, including dense myelinated axons, which helps explain the high density of oligodendrocytes, and to some extent astrocytes, in IM.

IM neurons and their roles in amygdala function

The distinct morphological and neurochemical classes of IM neurons also suggest different physiological properties and function. Neurons expressing DARPP-32 were spiny, similar to the medium-sized spiny neurons in the striatum (Anderson and Reiner, 1991; Ouimet et al., 1998), whereas the other two groups were aspiny. Our findings are in agreement with qualitative studies in several species that have described striatal-like medium-sized spiny neurons, as well as small and large NADPHd+, and CB+ neurons in IM (Millhouse, 1986; Nitecka and Ben-Ari, 1987; Sims and Williams, 1990; Pitkanen and Amaral, 1991, 1994; Barbas et al., 1993; McDonald and Augustine, 1993; Sorvari et al., 1996; Usunoff et al., 2006; Kaoru et al., 2010).

Differential distribution of DARPP-32 and NOS in IM suggests differences in the interactions of IM neurons with dopamine (Fienberg et al., 1998; Pape, 2005). Studies in the striatum have shown that under basal dopaminergic conditions, DARPP-32 is primarily phosphorylated at threonine75 (Thr75) and inhibits protein kinase A [(PKA); (Svenningsson et al., 2004)]. But under hyperdopaminergic conditions, phosphorylation at Thr75 is reduced and phosphorylation at Thr34 increases, with subsequent potentiation of dopaminergic signaling (Svenningsson et al., 2004). When DARPP-32 is phosphorylated at Thr34, it inhibits protein phosphatase inhibitor-1 and can amplify signaling mediated by protein kinases A and G (PKA, PKG). The PKA route involves dopamine acting through D1 receptors, which are enriched in IM [this study and (Fuxe et al., 2003; Pinto and Sesack, 2008; Muly et al., 2009; de la Mora et al., 2010)], consistent with the strong dopaminergic innervation of IM (Asan, 1997; Pape, 2005; Pinto and Sesack, 2008; Cho and Fudge, 2010). It is not clear, however, whether dopamine has the same effect on all types of IM neurons. For example, a study in mice has shown that dopamine can hyperpolarize IM paracapsular neurons through D1 receptors and substantially suppress their excitability, resulting in disinhibition of the basolateral and central nuclei (Marowsky et al., 2005).

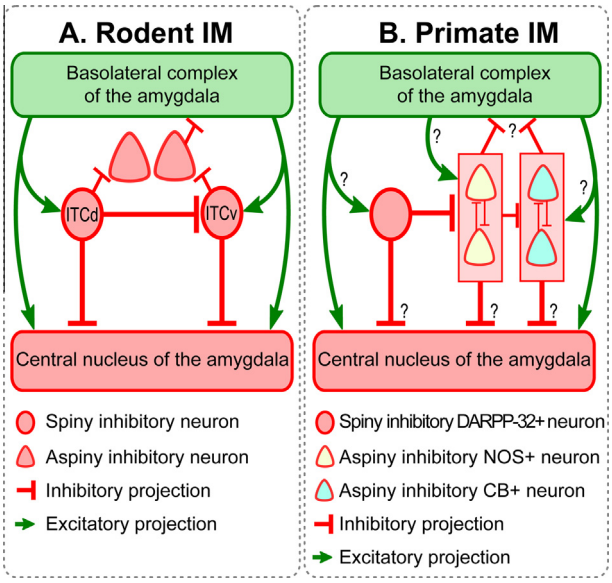

Fig. 13. Schematic diagrams showing (A) the rodent amygdala, and (B) the primate amygdala. ITCd: dorsal intercalated group located between BLA and Ce in rodents; ITCv: ventral intercalated group located between BLA and Ce in rodents. Similarities and differences in the connectivity of IM neurons are highlighted. Similarities between rodent and primate IM include the following: (1) Both contain small- and medium-sized spiny neurons that form clumps or clusters (circular cells). These clusters tend to be linked, creating continuous IM regions. In the rodent these regions are frequently divided into topographic regions. (2) Both contain larger aspiny neurons (triangular cells). (3) In both rodent and primate IM, aspiny neurons are inhibited by the smaller spiny neurons. Differences between rodent and primate IM include: (1) Rodent studies typically show interconnectivity among the spiny neuron groups. Here we show that the spiny DARPP-32+ neurons in primate IM are not interconnected, and only form synapses on the aspiny NOS+ neurons. (2) Rodent studies show that aspiny neurons surround the spiny IM clusters. Here we do not observe such clear-cut topographic separation between the spiny (DARPP-32+) and aspiny (NOS+ and CB+) neurons in IM. It may be more accurate to describe the two neuron groups as partially interspersed. (3) Aspiny neurons in rodents target BLA and extra-amygdalar regions, avoiding the parent IM region. In primates we observed instead a distinct pattern of inhibition among aspiny neurons. We observed that NOS neurons inhibit each other, as do CB neurons. NOS neurons also inhibit CB neurons. Thus instead of a topographically polarized pattern of inhibition, we observed intermingled neurons whose connectivity pattern was determined by neurochemical identity and showed no topographic polarization.

Another major factor that stimulates the phosphorylation of DARPP-32 at Thr34 is the NO/cGMP pathway through activation of PKG (Tsou et al., 1993). In the striatum of rats, blockage of NO or cGMP decreases responsiveness of striatal medium-sized spiny neurons (West and Grace, 2004). Combined, these findings highlight the critical role of DARPP-32 in the modulation of dopaminergic signaling as well as in significant interactions with multiple neurotransmitters and neuromodulators, including NO (Greengard, 2001; Svenningsson et al., 2004). Because NO is a gas, it can act outside direct synaptic interactions with significant anterograde and retrograde effects within local circuits (Bredt and Snyder, 1992; Snyder, 1992). In this context, acting as a retrograde (nonsynaptic) agent in the amygdalar IM, NO may help regulate DARPP-32 phosphorylation sites to enhance dopaminergic signaling. In addition, our findings suggest that through synaptic interactions DARPP-32+ neurons can anterogradely inhibit NOS+ neurons. Thus, the specific interactions of DARPP-32 and NOS neurons in the primate IM provide a mechanism for a signaling cascade for auto-regulation of the local circuit activity (Fig. 13B).

NO is involved in activity-dependent synaptic plasticity in several brain regions that play key roles in cognition and flexible, adaptive behavior (Prast and Philippu, 2001; Dachtler et al., 2011; Walton et al., 2013). In the amygdala, NO is additionally linked with modulation of anxiety levels and other emotional processes (Shindou et al., 1993; Yao et al., 2007). It should be noted that the largest neurons in the primate IM were NOS+, and a recent study showed that large IM neurons — which are distinct from small spiny IM neurons — relay noxious sensory information, and can innervate other inhibitory neurons in basal and lateral amygdalar nuclei (Bienvenu et al., 2015). This can transiently disinhibit principal neurons in the amygdala and facilitate the integration of aversive nociceptive inputs with neutral sensory stimuli, effectively participating in learning processes (Bienvenu et al., 2015)].

IM neurons and their roles in the amygdalar circuit: similarities and differences between rodents and rhesus monkeys

The amygdala is a central node of the limbic system, involved in emotional processing, motivation, and memory (Phelps, 2006; Murray, 2007; Pessoa, 2008; Morrison and Salzman, 2010; Pape and Pare, 2010; Pessoa and Adolphs, 2010; John et al., 2013; Paz and Pare, 2013; Lalumiere, 2014). The intra-amygdaloid circuit underlying these diverse functions is complex and includes the basal (BA) complex (also known as basolateral, BLA), the main input station of the amygdala for sensory afferents. The BLA ultimately connects with Ce, the major source of projections to brainstem structures, mediating fear and other emotional responses [reviewed in (Pare et al., 2003; Pape and Pare, 2010; Duvarci and Pare, 2014)]. Interposed between the two amygdalar regions, IM neurons can intercept excitatory projections from BLA and, in turn, inhibit Ce neurons. This general connectivity scheme seems to be preserved in mammals (Price and Amaral, 1981; De Olmos et al., 1985; De Olmos, 1990; McDonald, 1998; Fudge and Tucker, 2009; Pape and Pare, 2010; John et al., 2013).

In rodents, however, the topographic separation of distinct IM clusters underlies their distinct connectivity patterns and their specialized physiological properties and function. Fig. 13A shows the connectivity among IM neurons located between BLA and Ce [called ITCs or medial ITCs in some rodent studies; for discussion and model, see (John et al., 2013)]. Although there is evidence from rodents that the clusters of spiny neurons form a continuous neuronal net (Marowsky et al., 2005), investigators often divide the IM into three subpopulations, based on topography, function and connections (Royer et al., 2000a; de la Mora et al., 2010;

Amano et al., 2011; Busti et al., 2011; Li et al., 2011). At least two of these subpopulations appear to be crucial for fear conditioning and extinction (Busti et al., 2011; Li et al., 2011). The dorsolateral group (ITCd) is thought to inhibit the ventromedial group (ITCv) as well as the lateral subdivision of the central (CeL) amygdalar nucleus. The ventromedial group (ITCv), in turn, inhibits the medial subdivision of the central nucleus (CeM), which is the main amygdalar output to brainstem nuclei. Therefore, spiny neurons in the rodent IM are interconnected and are thought to gate signals between the BLA complex and Ce (Pare and Smith, 1993; Royer et al., 1999, 2000b; Likhtik et al., 2008; Manko et al., 2011).

Fig. 13B shows the proposed tentative connectivity among IM cells in the rhesus macaque, based on the quantitative ultrastructural study of synapses within the IM neuropil. Our results complement previous findings at the brightfield level that report robust inhibitory synaptic input in IM (McDonald and Augustine, 1993; Pitkanen and Amaral, 1994) and strong excitatory input, likely from the basal amygdalar nuclei, the thalamus, and cortex (McDonald, 1998; McDonald et al., 1999; Ghashghaei and Barbas, 2002; Pare et al., 2003; Quirk et al., 2003; Berretta et al., 2005; Rempel-Clower, 2007; Amano et al., 2010; Pinard et al., 2012; Strobel et al., 2015). Significantly, our data show that primates do not possess topographically distinct subpopulations of spiny IM neurons that inhibit each other. Instead, we found three neurochemically distinct classes of inhibitory neurons that are intermingled in an unbroken IM continuum. These neurons expressed respectively DARPP-32, NOS/NADPH, or the calcium-binding protein CB. Within the IM neuropil, the spiny DARPP-32+ neurons formed synapses with the aspiny NOS/NADPH+ neurons. We found no evidence of synaptic interactions between spiny neurons, as reported for rodents. Our data therefore, suggest that the interconnectivity of IM neurons in primates is likely neurochemically specific and not spatially polarized, as reported for rodents.

Rodent IM studies report that groups of aspiny neurons surround the spiny neuron clusters (McDonald and Mascagni, 2011; Bienvenu et al., 2015), and are targeted by the spiny neurons (Busti et al., 2011), which is in line with some of our observations in primates. Further, in rodents the axons of the aspiny neurons reportedly avoid the parent IM regions, targeting the BLA and also regions outside the amygdala (Bienvenu et al., 2015). In contrast, we found that in rhesus monkeys mutual inhibition between neurons that belong to the same neurochemical group is only observed within the two putative aspiny groups: the NOS+ and the CB+ neurons. In addition, the NOS+ neurons innervate CB + neurons (Fig. 13). Moreover, unlike observations in rodents (Bienvenu et al., 2015), we found no IM neurons positive for PV, in agreement with previous studies in monkeys and humans (Pitkanen and Amaral, 1993; Sorvari et al., 1995; Ghashghaei and Barbas, 2002; Pantazopoulos et al., 2006). Thus the intrinsic circuitry in primate IM may differ from the rodent. These findings suggest species-specific differences in inhibitory dynamics that reflect variable or bistable behavior of IM neurons (Pare et al., 2003; Catterall and Few, 2008; Camp and Wijesinghe, 2009; Lohmann, 2009).

More physiologic and anatomic studies are needed to establish the entire complement of the sources of inputs onto these inhibitory neurons. It is thus necessary to investigate further to what extent the polarized connectivity of IM neurons reflects interconnectivity within IM, and what is the contribution from other amygdalar nuclei or other structures that have some of the same inhibitory neurons and also innervate the IM.

CONCLUSIONS

We highlighted remarkable histochemical and structural specificity of IM neurons and their circuits in rhesus monkeys. These features likely underlie the functional specialization and diverse contribution of IM neurons in learning and emotional processing. The neurochemical and functional specificity of IM neurons, along with their intricate interconnections and preferential targeting by the posterior orbitofrontal cortex (Ghashghaei and Barbas, 2002; Barbas et al., 2011), allow for flexible, context-dependent gating of intra- and extra-amygdalar traffic. These circuits are associated with acquisition or extinction of fear and complex emotional processes that are disrupted in anxiety disorders.

Acknowledgments—We thank Dr. Alan Peters for EM consultation, Dr. John Fiala for assistance in adapting the free 3D-reconstruction software he developed, Drs. Ron Killiany, Maria Medalla and Clare Timbie for MRI and surgical assistance, Drs. Paul Greengard and Jean-Antoine Girault for their generous gift of the DARPP-32 antibody, and Mrs. Marcia Feinberg for exceptional technical assistance and imaging at the electron microscope. Supported by grants from NIH (BZ: R01 MH101209, HB: R01 MH057414, R01 NS024760) and NSF CELEST (YJ, HB, BZ: 0835976).

REFERENCES

Amano T, Duvarci S, Popa D, Pare D (2011) The fear circuit revisited: contributions of the basal amygdala nuclei to conditioned fear. J Neurosci 31:15481–15489.

Amano T, Unal CT, Pare D (2010) Synaptic correlates of fear extinction in the amygdala. Nat Neurosci 13:489–494.

Amaral DG, Price JL, Pitkanen A, Carmichael ST (1992) The Amygdala: neurobiological aspects of emotion, memory, and mental dysfunction. New York: Wiley-Liss.

Anderson KD, Reiner A (1991) Immunohistochemical localization of DARPP-32 in striatal projection neurons and striatal interneurons: implications for the localization of D1-like dopamine receptors on different types of striatal neurons. Brain Res 568:235–243.

Asan E (1997) Ultrastructural features of tyrosine-hydroxylase-immunoreactive afferents and their targets in the rat amygdala. Cell Tissue Res 288:449–469.

Asede D, Bosch D, Luthi A, Ferraguti F, Ehrlich I (2015) Sensory inputs to intercalated cells provide fear-learning modulated inhibition to the basolateral amygdala. Neuron 86:541–554.

Barbas H, De Olmos J (1990) Projections from the amygdala to basoventral and mediodorsal prefrontal regions in the rhesus monkey. J Comp Neurol 300:549–571.

Barbas H, Gustafson EL, Greengard P (1993) Comparison of the immunocytochemical localization of DARPP-32 and I-1 in the amygdala and hippocampus of the rhesus monkey. J Comp Neurol 334:1–18.

Barbas H, Medalla M, Alade O, Suski J, Zikopoulos B, Lera P (2005) Relationship of prefrontal connections to inhibitory systems in superior temporal areas in the rhesus monkey. Cereb Cortex 15:1356–1370.

Barbas H, Zikopoulos B, Timbie C (2011) Sensory pathways and emotional context for action in primate prefrontal cortex. Biol Psychiatry 69:1133–1139.

Berretta S, Pantazopoulos H, Caldera M, Pantazopoulos P, Pare D (2005) Infralimbic cortex activation increases c-Fos expression in intercalated neurons of the amygdala. Neuroscience 132:943–953.

Bienvenu TC, Busti D, Micklem BR, Mansouri M, Magill PJ, Ferraguti F, Capogna M (2015) Large intercalated neurons of amygdala relay noxious sensory information. J Neurosci 35:2044–2057.

Blazquez-Llorca L, Garcia-Marin V, DeFelipe J (2010) GABAergic complex basket formations in the human neocortex. J Comp Neurol 518:4917–4937.

Bredt DS, Snyder SH (1992) Nitric oxide, a novel neuronal messenger. Neuron 8:3–11.

Busti D, Geracitano R, Whittle N, Dalezios Y, Manko M, Kaufmann W, Satzler K, Singewald N, Capogna M, Ferraguti F (2011) Different fear states engage distinct networks within the intercalated cell clusters of the amygdala. J Neurosci 31:5131–5144.

Camp AJ, Wijesinghe R (2009) Calretinin: modulator of neuronal excitability. Int J Biochem Cell Biol 41:2118–2121.

Capogna M (2014) GABAergic cell type diversity in the basolateral amygdala. Curr Opin Neurobiol 26:110–116.

Carlo CN, Stefanacci L, Semendeferi K, Stevens CF (2010) Comparative analyses of the neuron numbers and volumes of the amygdaloid complex in old and new world primates. J Comp Neurol 518:1176–1198.

Catterall WA, Few AP (2008) Calcium channel regulation and presynaptic plasticity. Neuron 59:882–901.

Chareyron LJ, Banta Lavenex P, Amaral DG, Lavenex P (2011) Stereological analysis of the rat and monkey amygdala. J Comp Neurol 519:3218–3239.

Cho YT, Fudge JL (2010) Heterogeneous dopamine populations project to specific subregions of the primate amygdala. Neuroscience 165:1501–1518.

Crosby EC, Humphrey T (1941) Studies of the vertebrate telencephalon. II. The nuclear pattern of the anterior olfactory nucleus tuberculum olfactorium and the amygdaloid complex in adult man. J Comp Neurol 74:309–352.

Dachtler J, Hardingham NR, Glazewski S, Wright NF, Blain EJ, Fox K (2011) Experience-dependent plasticity acts via GluR1 and a novel neuronal nitric oxide synthase-dependent synaptic mechanism in adult cortex. J Neurosci 31:11220–11230.

de la Mora MP, Gallegos-Cari A, Arizmendi-Garcia Y, Marcellino D, Fuxe K (2010) Role of dopamine receptor mechanisms in the amygdaloid modulation of fear and anxiety: Structural and functional analysis. Prog Neurobiol 90:198–216.

De Olmos J (1990) Amygdaloid nuclear gray complex. In: Paxinos G, editor. The human nervous system. San Diego (CA): Acedemic Press Inc. p. 583–710.

De Olmos J, Alheid GF, Beltramino CA (1985) Amygdala. In: Paxinos G, editor. The rat nervous system. Sydney, Australia: Academic Press. p. 223–333.

De Olmos JS, Heimer L (1999) The concepts of the ventral striatopallidal system and extended amygdala. Ann N Y Acad Sci 877:1–32.

del Río-Hortega P (1919) El tercer elemento de los centros nerviosos. I La microglía en estado normal. Bol Soc Esp Biol 9:68–169.

del Río-Hortega P (1921) Estudios sobre la neuroglía. La glía de escasas radiaciones (oligodendroglía). Bol R Soc Esp Hist Nat 21:63–92.

del Río-Hortega P (1928) Tercera aportación al conocimiento morfológico e interpretación funcional de la oligodendroglía. Mem R Soc Esp Hist Nat 14:5–122.

del Río-Hortega P (1932) Microglia. In: Penfield W, editor. Cytology and cellular pathology of the nervous system, Vol. II. New York: Paul B. Hoebner Inc. p. 481–534.

Dombrowski SM, Barbas H (1996) Differential expression of NADPH diaphorase in functionally distinct prefrontal cortices in the rhesus monkey. Neuroscience 72:49–62.

Duvarci S, Pare D (2014) Amygdala microcircuits controlling learned fear. Neuron 82:966–980.

Emery NJ, Capitanio JP, Mason WA, Machado CJ, Mendoza SP, Amaral DG (2001) The effects of bilateral lesions of the amygdala on dyadic social interactions in rhesus monkeys (Macaca mulatta). Behav Neurosci 115:515–544.

Fiala JC (2005) Reconstruct: a free editor for serial section microscopy. J Microsc 218:52–61.

Fienberg AA, Hiroi N, Mermelstein PG, Song W, Snyder GL, Nishi A, Cheramy A, O'Callaghan JP, Miller DB, Cole DG, Corbett R, Haile CN, Cooper DC, Onn SP, Grace AA, Ouimet CC, White FJ, Hyman SE, Surmeier DJ, Girault J, Nestler EJ, Greengard P (1998) DARPP-32: regulator of the efficacy of dopaminergic neurotransmission. Science 281:838–842.

Fudge JL, Tucker T (2009) Amygdala projections to central amygdaloid nucleus subdivisions and transition zones in the primate. Neuroscience 159:819–841.

Fuxe K, Jacobsen KX, Hoistad M, Tinner B, Jansson A, Staines WA, Agnati LF (2003) The dopamine D1 receptor-rich main and paracapsular intercalated nerve cell groups of the rat amygdala: relationship to the dopamine innervation. Neuroscience 119:733–746.

Gabbott PL, Stewart MG (1987) Distribution of neurons and glia in the visual cortex (area 17) of the adult albino rat: a quantitative description. Neuroscience 21:833–845.

García-Cabezas MA, Barbas H (2014) Area 4 has layer IV in adult primates. Eur J Neurosci 39:1824–1834.

Ghashghaei HT, Barbas H (2002) Pathways for emotion: Interactions of prefrontal and anterior temporal pathways in the amygdala of the rhesus monkey. Neuroscience 115:1261–1279.

Greengard P (2001) The neurobiology of slow synaptic transmission. Science 294:1024–1030.

Gundersen HJ (1986) Stereology of arbitrary particles. A review of unbiased number and size estimators and the presentation of some new ones, in memory of William R. Thompson. J Microsc 143(Pt 1):3–45.

Hashikawa T, Leggio MG, Hattori R, Yuri Y (1994) Nitric oxide synthase immunoreactivity colocalized with NADPH-diaphorase histochemistry in the monkey cerebral cortex. Brain Res 641:341–349.

Heimer L (2003) A new anatomical framework for neuropsychiatric disorders and drug abuse. Am J Psychiatry 160:1726–1739.

Hope BT, Michael GL, Knigge KM, Vincent SR (1991) Neuronal NADPH diaphorase is a nitric oxide synthase. Proc Natl Acad Sci U S A 88:2811–2814.

Howard CV, Reed MG (1998) Unbiased stereology, three-dimensional measurement in microscopy. Oxford (UK): BIOS Scientific Publishers Limited.

John YJ, Bullock D, Zikopoulos B, Barbas H (2013) Anatomy and computational modeling of networks underlying cognitive-emotional interaction. Front Hum Neurosci 7:101.

Kaoru T, Liu FC, Ishida M, Oishi T, Hayashi M, Kitagawa M, Shimoda K, Takahashi H (2010) Molecular characterization of the intercalated cell masses of the amygdala: implications for the relationship with the striatum. Neuroscience 166:220–230.

Lalumiere RT (2014) Optogenetic dissection of amygdala functioning. Front Behav Neurosci 8:107.

Li GS, Amano T, Pare D, Nair SS (2011) Impact of infralimbic inputs on intercalated amygdala neurons: A biophysical modeling study. Learning & Memory 18:226–240.

Likhtik E, Paz R (2015) Amygdala-prefrontal interactions in (mal) adaptive learning. Trends Neurosci 38:158–166.

Likhtik E, Popa D, Apergis-Schoute J, Fidacaro GA, Pare D (2008) Amygdala intercalated neurons are required for expression of fear extinction. Nature 454:642–645.

Ling EA, Paterson JA, Privat A, Mori S, Leblond CP (1973) Investigation of glial cells in semithin sections. I. Identification of glial cells in the brain of young rats. J Comp Neurol 149:43–71.

Lohmann C (2009) Calcium signaling and the development of specific neuronal connections. Prog Brain Res 175:443–452.
Manko M, Geracitano R, Capogna M (2011) Functional connectivity of the main intercalated nucleus of the mouse amygdala. J Physiol 589:1911–1925.
Marcellino D, Frankowska M, Agnati L, Perez de la Mora M, Vargas-Barroso V, Fuxe K, Larriva-Sahd J (2012) Intercalated and paracapsular cell islands of the adult rat amygdala: a combined rapid-Golgi, ultrastructural, and immunohistochemical account. Neuroscience 226:324–347.
Maren S, Phan KL, Liberzon I (2013) The contextual brain: implications for fear conditioning, extinction and psychopathology. Nat Rev Neurosci 14:417–428.
Marin-Padilla M (1970) Prenatal and early postnatal ontogenesis of the human motor cortex: a golgi study. II. The basket-pyramidal system. Brain Res 23:185–191.
Marowsky A, Yanagawa Y, Obata K, Vogt KE (2005) A specialized subclass of interneurons mediates dopaminergic facilitation of amygdala function. Neuron 48:1025–1037.
McDonald AJ (1998) Cortical pathways to the mammalian amygdala. Prog Neurobiol 55:257–332.
McDonald AJ, Augustine JR (1993) Localization of GABA-like immunoreactivity in the monkey amygdala. Neuroscience 52:281–294.
McDonald AJ, Mascagni F (2011) Neuronal localization of M2 muscarinic receptor immunoreactivity in the rat amygdala. Neuroscience 196:49–65.
McDonald AJ, Shammah-Lagnado SJ, Shi C, Davis M (1999) Cortical afferents to the extended amygdala. Ann N Y Acad Sci 877:309–338.
Medalla M, Barbas H (2006) Diversity of laminar connections linking periarcuate and lateral intraparietal areas depends on cortical structure. Eur J Neurosci 23:161–179.
Medalla M, Barbas H (2009) Synapses with inhibitory neurons differentiate anterior cingulate from dorsolateral prefrontal pathways associated with cognitive control. Neuron 61:609–620.
Medalla M, Barbas H (2012) The anterior cingulate cortex may enhance inhibition of lateral prefrontal cortex via m2 cholinergic receptors at dual synaptic sites. J Neurosci 32:15611–15625.
Millhouse OE (1986) The intercalated cells of the amygdala. J Comp Neurol 247:246–271.
Morrison SE, Salzman CD (2010) Re-valuing the amygdala. Curr Opin Neurobiol 20:221–230.
Mosher CP, Zimmerman PE, Gothard KM (2010) Response characteristics of basolateral and centromedial neurons in the primate amygdala. J Neurosci 30:16197–16207.
Muly EC, Senyuz M, Khan ZU, Guo JD, Hazra R, Rainnie DG (2009) Distribution of D1 and D5 dopamine receptors in the primate and rat basolateral amygdala. Brain Struct Funct 213:375–393.
Murray EA (2007) The amygdala, reward and emotion. Trends Cogn Sci 11:489–497.
Murray EA, Wise SP, Drevets WC (2011) Localization of dysfunction in major depressive disorder: prefrontal cortex and amygdala. Biol Psychiatry 69:e43–e54.
Nitecka L, Ben-Ari Y (1987) Distribution of GABA-like immunoreactivity in the rat amygdaloid complex. J Comp Neurol 266:45–55.
O'Kusky J, Colonnier M (1982) A laminar analysis of the number of neurons, glia, and synapses in the visual cortex (area 17) of adult macaque monkeys. J Comp Neurol 210:278–290.
Ouimet CC, Langley-Gullion KC, Greengard P (1998) Quantitative immunocytochemistry of DARPP-32-expressing neurons in the rat caudatoputamen. Brain Res 808:8–12.
Palomares-Castillo E, Hernandez-Perez OR, Perez-Carrera D, Crespo-Ramirez M, Fuxe K, Perez de la Mora M (2012) The intercalated paracapsular islands as a module for integration of signals regulating anxiety in the amygdala. Brain Res 1476:211–234.
Pantazopoulos H, Lange N, Hassinger L, Berretta S (2006) Subpopulations of neurons expressing parvalbumin in the human amygdala. J Comp Neurol 496:706–722.
Pape HC (2005) GABAergic neurons: gate masters of the amygdala, mastered by dopamine. Neuron 48:877–879.
Pape HC, Pare D (2010) Plastic Synaptic Networks of the Amygdala for the Acquisition, Expression, and Extinction of Conditioned Fear. Physiol Rev 90:419–463.
Pare D, Quirk GJ, LeDoux JE (2004) New vistas on amygdala networks in conditioned fear. J Neurophysiol 92:1–9.
Pare D, Royer S, Smith Y, Lang EJ (2003) Contextual inhibitory gating of impulse traffic in the intra-amygdaloid network. Ann N Y Acad Sci 985:78–91.
Pare D, Smith Y (1993) The intercalated cell masses project to the central and medial nuclei of the amygdala in cats. Neuroscience 57:1077–1090.
Paz R, Pare D (2013) Physiological basis for emotional modulation of memory circuits by the amygdala. Curr Opin Neurobiol 23:381–386.
Pessoa L (2008) On the relationship between emotion and cognition. Nat Rev Neurosci 9:148–158.
Pessoa L, Adolphs R (2010) Emotion processing and the amygdala: from a 'low road' to 'many roads' of evaluating biological significance. Nat Rev Neurosci 11:773–783.
Peters A, Palay S (1996) The morphology of synapses. J Neurocytol 25:687–700.
Peters A, Palay SL, Webster HD (1991) The fine structure of the nervous system. Neurons and their supporting cells. New York (NY): Oxford University Press.
Peters A, Verderosa A, Sethares C (2008) The neuroglial population in the primary visual cortex of the aging rhesus monkey. Glia 56:1151–1161.
Phelps EA (2006) Emotion and cognition: insights from studies of the human amygdala. Annu Rev Psychol 57:27–53.
Phillips ML, Drevets WC, Rauch SL, Lane R (2003) Neurobiology of emotion perception II: Implications for major psychiatric disorders. Biol Psychiatry 54:515–528.
Pinard CR, Mascagni F, McDonald AJ (2012) Medial prefrontal cortical innervation of the intercalated nuclear region of the amygdala. Neuroscience 205:112–124.
Pinto A, Sesack SR (2008) Ultrastructural analysis of prefrontal cortical inputs to the rat amygdala: spatial relationships to presumed dopamine axons and D1 and D2 receptors. Brain Struct Funct 213:159–175.
Pitkanen A, Amaral DG (1991) Distribution of reduced nicotinamide adenine dinucleotide phosphate diaphorase (NADPH-d) cells and fibers in the monkey amygdaloid complex. J Comp Neurol 313:326–348.
Pitkanen A, Amaral DG (1993) Distribution of parvalbumin-immunoreactive cells and fibers in the monkey temporal lobe: the amygdaloid complex. J Comp Neurol 331:14–36.
Pitkanen A, Amaral DG (1994) The distribution of GABAergic cells, fibers, and terminals in the monkey amygdaloid complex: an immunohistochemical and *in situ* hybridization study. J Neurosci 14:2200–2224.
Pitkanen A, Amaral DG (1998) Organization of the intrinsic connections of the monkey amygdaloid complex: projections originating in the lateral nucleus. J Comp Neurol 398: 431–458.
Prast H, Philippu A (2001) Nitric oxide as modulator of neuronal function. Prog Neurobiol 64:51–68.
Price JL (2003) Comparative aspects of amygdala connectivity. Ann N Y Acad Sci 985:50–58.
Price JL, Amaral DG (1981) An autoradiographic study of the projections of the central nucleus of the monkey amygdala. J Neurosci 1:1242–1259.
Quirk GJ, Gehlert DR (2003) Inhibition of the amygdala: key to pathological states? Ann N Y Acad Sci 985:263–272.
Quirk GJ, Likhtik E, Pelletier JG, Pare D (2003) Stimulation of medial prefrontal cortex decreases the responsiveness of central amygdala output neurons. J Neurosci 23:8800–8807.
Ramón y Cajal S (1896) Estructura del protoplama nervioso. Rev Trim Microg 1:1–30.

Ramón y Cajal S. (1899/2002). Textura del sistema nervioso del hombre y de los vertebrados. Tomo I. Zaragoza: Gobierno de Aragón. Departamento de Cultura y Turismo.
Ramón y Cajal S (1913) Contribución al conocimiento de la neuroglia del cerebro humano. Trab Lab Invest Biol 11:255–315.
Rempel-Clower NL (2007) Role of orbitofrontal cortex connections in emotion. Ann N Y Acad Sci 1121:72–86.
Rosene DL, Roy NJ, Davis BJ (1986) A cryoprotection method that facilitates cutting frozen sections of whole monkey brains from histological and histochemical processing without freezing artifact. J Histochem Cytochem 34:1301–1315.
Royer S, Martina M, Pare D (1999) An inhibitory interface gates impulse traffic between the input and output stations of the amygdala. J Neurosci 19:10575–10583.
Royer S, Martina M, Pare D (2000a) Bistable behavior of inhibitory neurons controlling impulse traffic through the amygdala: role of a slowly deinactivating K+ current. J Neurosci 20: 9034–9039.
Royer S, Martina M, Pare D (2000b) Polarized synaptic interactions between intercalated neurons of the amygdala. J Neurophysiol 83:3509–3518.
Sah P, Faber ES, Lopez DA, Power J (2003) The amygdaloid complex: anatomy and physiology. Physiol Rev 83:803–834.
Schindelin J, Arganda-Carreras I, Frise E, Kaynig V, Longair M, Pietzsch T, Preibisch S, Rueden C, Saalfeld S, Schmid B, Tinevez JY, White DJ, Hartenstein V, Eliceiri K, Tomancak P, Cardona A (2012) Fiji: an open-source platform for biological-image analysis. Nat Methods 9:676–682.
Shin LM, Rauch SL, Pitman RK (2006) Amygdala, medial prefrontal cortex, and hippocampal function in PTSD. Ann N Y Acad Sci 1071:67–79.
Shindou T, Watanabe S, Yamamoto K, Nakanishi H (1993) NMDA receptor-dependent formation of long-term potentiation in the rat medial amygdala neuron in an *in vitro* slice preparation. Brain Res Bull 31:667–672.
Sims KS, Williams RS (1990) The human amygdaloid complex: a cytologic and histochemical atlas using Nissl, myelin, acetylcholinesterase and nicotinamide adenine dinucleotide phosphate diaphorase staining. Neuroscience 36:449–472.
Snyder SH (1992) Nitric oxide: First in a new class of neurotransmitters? Science 257:494–496.
Sorvari H, Soininen H, Paljarvi L, Karkola K, Pitkanen A (1995) Distribution of parvalbumin-immunoreactive cells and fibers in the human amygdaloid complex. J Comp Neurol 360:185–212.
Sorvari H, Soininen H, Pitkanen A (1996) Calbindin-D28K-immunoreactive cells and fibres in the human amygdaloid complex. Neuroscience 75:421–443.
Stephan H, Andy OJ (1977) Quantitative comparison of the amygdala in insectivores and primates. Acta Anatomica 98:130–153.
Strobel C, Marek R, Gooch HM, Sullivan RK, Sah P (2015) Prefrontal and auditory input to intercalated neurons of the amygdala. Cell Rep.
Svenningsson P, Nishi A, Fisone G, Girault JA, Nairn AC, Greengard P (2004) DARPP-32: An integrator of neurotransmission. Ann Rev Pharmacol Toxicol 44:269–296.
Timbie C, Barbas H (2014) Specialized pathways from the primate amygdala to posterior orbitofrontal cortex. J Neurosci 34:8106–8118.
Timbie C, Barbas H (2015) Pathways for emotions: Specializations in the amygdalar, mediodorsal thalamic, and posterior orbitofrontal network. J Neurosci 35:11976–11987.
Tsou K, Snyder GL, Greengard P (1993) Nitric oxide/cGMP pathway stimulates phosphorylation of DARPP-32, a dopamine- and cAMP-regulated phosphoprotein, in the substantia nigra. Proc Natl Acad Sci U S A 90:3462–3465.
Tye KM, Prakash R, Kim SY, Fenno LE, Grosenick L, Zarabi H, Thompson KR, Gradinaru V, Ramakrishnan C, Deisseroth K (2011) Amygdala circuitry mediating reversible and bidirectional control of anxiety. Nature 471:358–362.
Urban S, Yilmazer-Hanke DM (1999) The pigmentarchitectonic divisions and neuronal types of the central nucleus and intercalated masses of the human amygdala1. J Hirnforsch 39:311–319.
Usunoff KG, Itzev DE, Rolfs A, Schmitt O, Wree A (2006) Nitric oxide synthase-containing neurons in the amygdaloid nuclear complex of the rat. Anat Embryol (Berl) 211:721–737.
Waclaw RR, Ehrman LA, Pierani A, Campbell K (2010) Developmental origin of the neuronal subtypes that comprise the amygdalar fear circuit in the mouse. J Neurosci 30:6944–6953.
Walton JC, Selvakumar B, Weil ZM, Snyder SH, Nelson RJ (2013) Neuronal nitric oxide synthase and NADPH oxidase interact to affect cognitive, affective, and social behaviors in mice. Behav Brain Res 256:320–327.
West AR, Grace AA (2004) The nitric oxide-guanylyl cyclase signaling pathway modulates membrane activity states and electrophysiological properties of striatal medium spiny neurons recorded *in vivo*. J Neurosci 24:1924–1935.
Wolff SB, Grundemann J, Tovote P, Krabbe S, Jacobson GA, Muller C, Herry C, Ehrlich I, Friedrich RW, Letzkus JJ, Luthi A (2014) Amygdala interneuron subtypes control fear learning through disinhibition. Nature 509:453–458.
Yao ST, Antunes VR, Paton JF, Murphy D (2007) Osmotic regulation of neuronal nitric oxide synthase expression in the rat amygdala: functional role for nitric oxide in adaptive responses? J Neurosci Res 85:410–422.
Zikopoulos B, Barbas H (2006) Prefrontal projections to the thalamic reticular nucleus form a unique circuit for attentional mechanisms. J Neurosci 26:7348–7361.
Zikopoulos B, Barbas H (2007) Parallel driving and modulatory pathways link the prefrontal cortex and thalamus. PLoS One 2 e848.
Zikopoulos B, Barbas H (2012) Pathways for emotions and attention converge on the thalamic reticular nucleus in primates. J Neurosci 32:5338–5350.

(Accepted 26 May 2016)
(Available online 30 May 2016)